CHAPTER 2

Peptide amphiphiles: a comparison of the self-assembly behavior exhibited by conventional and thiolated analogues

2.1 Abstract

Peptide amphiphiles self-assemble in solution into an array of three-dimensional structures, while at interfaces two-dimensional structures are formed. This makes peptide amphiphiles a potentially attractive stabilizing coating for gold nanoparticles enabling future applications in biomedical fields like imaging and theranostics. For this, peptide amphiphiles must be functionalized with a thiol group to covalent facilitate attachment to the gold surface. Peptide amphiphiles usually comprise a peptidic headgroup conjugated to an alkyl chain. Small changes in their structure, for example alterations in peptide composition or modifications to the alkyl chain, including changes in length or the introduction of a thiol group, can lead to significant changes in the morphology of the resulting self-assembled structures. In this chapter, a range of amphiphiles with different peptide sequences, alkyl chain lengths, and with or without a terminal thiol are designed, synthesized and characterized to determine which amphiphiles demonstrate self-assembly behavior appropriate to stabilize gold nanoparticles.

2.2 Introduction

To date there is still a need to develop colloidally stable gold nanoparticles (GNPs) that are easy-to-functionalize, biocompatible, and suitable for biological applications. GNPs are typically synthesized with a citrate coating as a stabilizer, which is unstable under physiological conditions and a different coating is therefore required.[1, 2] Polymers[3-5] or silica[6-8] coatings are commonly used for this purpose.[5] However, the size of the GNPs is often significantly increased due to the thickness of these coatings.[8] Therefore, low molecular weight molecules are also studied as a GNP stabilizer. Among others,[9, 10] oligopeptides are able to stabilize small spherical GNPs (≤30 nm). These peptides tether to a gold surface *via* the cysteine side chain resulting in covalent binding through Au-S bond formation.[11, 12] The stabilizing effect of these peptides was partially attributed to their propensity to self-assemble into β-structures both in solution and when attached to a gold surface.[13, 14] Peptide backbones arrange perpendicularly to the gold surface and are held in place by intermolecular hydrogen bonding and hydrophobic interactions resulting in self-assembled monolayers (SAMs). However, these peptides also have limitations: their use for coating larger GNPs or GNPs of other shapes than spherical has not been reported.

To overcome the limitations of cysteine-containing peptides as GNP stabilizers, a new design based on peptide amphiphiles is suggested in this thesis. Peptide amphiphiles are a class of self-assembling materials and composed of a (polar) peptide segment conjugated to an aliphatic chain.[15] This molecule type differs from amphiphilic peptides, which are also capable of forming self-assembled structures either due to the presence of

hydrophobic and hydrophilic peptide blocks,[16] or due to the alternating order of hydrophobic and hydrophilic amino acid residues.[17]

Peptide amphiphiles are designed to form well-defined supramolecular structures in aqueous conditions. The driving force is hydrophobic collapse by sequestering the alkyl chains from the solvent to form the core of the supramolecular structure, and ordered secondary structure formation as a result of intermolecular hydrogen bonding by the peptide segment.[18] Additionally, these amphiphiles usually are (partially) charged thereby increasing solubility and the electrostatic repulsion at the periphery of the assembly prevents aggregation.[15] Peptide amphiphiles can be designed *de novo*, or inspired by example from Nature (e.g. toll-like receptor motifs with multiple alkyl chains attached to a single peptide domain).[19]

If a thiol group is introduced at the terminus of the amphiphile's alkyl chain, it is possible to tether these molecules on a gold surface *via* an Au-S bond. In this arrangement the gold core is surrounded with a hydrophobic environment created by the alkyl chains, therefore shielding the gold surface from undesired interactions with the biological medium. Also, the charged surface of peptide amphiphile-based supramolecular structures, increases the colloidal stability of coated GNPs due to the increased repulsive forces.[11] Additionally, a high propensity to form β-sheets, typical for peptide amphiphiles, is an advantage for a GNP stabilizer. There are three variables affecting peptide amphiphiles self-assembly in aqueous media or on a surface: the alkyl chain (*e.g.* length, degree of unsaturation, and functional groups like thiol), the amino acid sequence within the peptide domain, and the net charge. Previously it was shown that altering one of these components can already have a significant effect on the self-assembly behavior.[18, 20-22] Typically, peptide amphiphiles in solution assemble into

micelles and fibers. However, other morphologies including nanoribbons and nanobelts, or 1D fibers that align into more complex structures are also observed (**Scheme 2.1**).[15]

Alkyl chains spanning a length range from 6-24 carbon atoms have been used to control peptide amphiphile assembly. The results of these collective studies were presented in an elaborate review by Hamley.[23] The minimum alkyl chain length required to induce formation of a supramolecular structure has been discussed in several studies.[24] Alterations made to the alkyl chain define the stability of the supramolecular structures formed though the molecule's geometry. In some cases, it is favourable to use shorter alkyl chains as they do not interfere with the peptide self-assembly behavior, therefore maintaining the peptide-driven mode of self-assembly.[25]

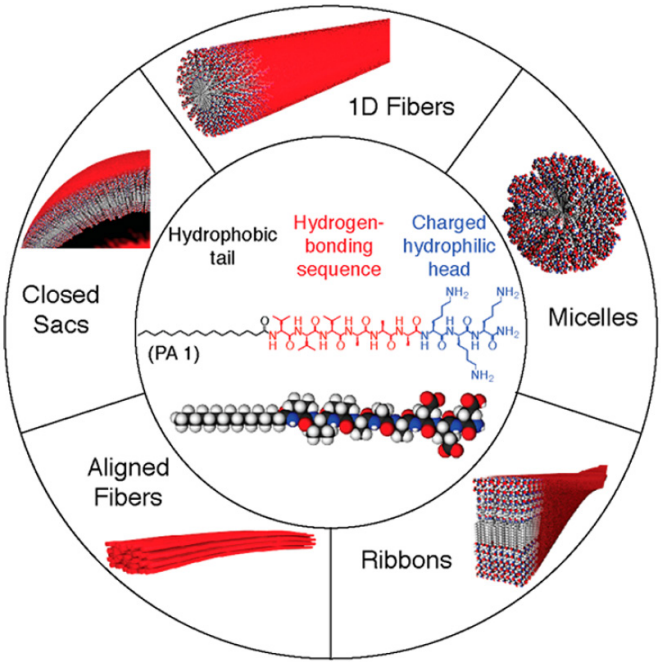

Scheme 2.1. Schematic explanation of different morphologies that can be formed by peptide amphiphiles (a generic amphiphile structure is shown in the middle). Image adapted from reference 15.

The primary amino acid sequence of peptide amphiphiles is always a combination of non-polar residues such as alanine (Ala, A), valine (Val, V), leucine (Leu, L), isoleucine (Ile, I), or phenylalanine (Phe, F), and charged residues including lysine (Lys, K), arginine (Arg, R), glutamic acid (Glu, E), or aspartic acid (Asp, D).[15, 23, 26]. The steric bulk of the side chains is important for both non-polar and charged residues, since it defines the molecule's geometry and self-assembly propensity. Numerous studies have reported how the amino acid sequence influences the self-assembly of peptide amphiphiles.[23, 26]. Stupp and coworkers observed that, for higher-order self-assembly into supramolecular fibers, it is beneficial to have longer peptide domains comprising more non-polar residues in comparison to charged residues, with bulky non-polar residues directly conjugated to a palmitoyl (C16) alkyl chain. This is due to hydrogen bond alignment being more effective when bulky residues are located next to the hydrophobic core.[18] In this study, the sequence palmitoyl-$V_4A_2E_3$ was the best-performing sequence as it demonstrated the highest β-sheet propensity. The composition of the peptide domain also influences the dynamic exchange of monomers between the supramolecular fibers as was revealed by Stochastic optical reconstruction microscopy (STORM).[27] Palmitoyl-$A_3G_3K_3$ assemblies showed to be more dynamic and flexible compared to palmitoyl-$V_3A_3K_3$ affecting the viability of cells cultured on these materials.[28] It was shown that flexible peptide amphiphiles cause cell death. Furthermore, reducing the amino acid residue number has also an impact on the resulting assemblies: palmitoyl-$V_3A_3E_3$ assembled into cylindrical fibers, while palmitoyl-$V_2A_2E_3$ yielded twisted nanoribbons.[29]

Peptide amphiphile assemblies are responsive to both the pH and ionic strength of the solution. For example, lowering the pH led to protonation of Glu residues in palmitoyl-I-A_3E_4-NH_2 resulting in a decrease in electrostatic

repulsion and a concomitant morphology change from spherical micelles to fibers with a predominantly β-sheet structure.[30] In another example, increasing the pH of a palmitoyl-VEVE solution led to a rearrangement of supramolecular sheets into nanobelts.[31, 32] Interestingly, the same peptide amphiphile showed three distinctly different arrangements at different concentrations: twisted nanoribbons at 0.01 wt%, a “broom”-like morphology at 0.05 wt%, and nanobelts at 0.1 wt%.[31]

The ionic strength has also a pronounced effect on peptide amphiphile assembly. Repulsion between positively charged Lys residues in palmitoyl-$V_3A_3K_3$ decreases when the ionic strength increases leading to charge screening and enhanced β-sheet formation.[33] Addition of divalent salts (*e.g.* $CaCl_2$) led to a transformation of the palmitoyl-$V_3A_3E_3$ peptide amphiphile solution into a gel.[34, 35] In a different approach, combining two peptide amphiphiles with opposite charge, leads to the formation of a mixed fiber exhibiting decreased thermal stability.[20]

In summary, these examples prove that many factors influence the self-assembly behavior of peptide amphiphiles, including the peptide amphiphile chemical composition, and external factors such as changes in the peptide amphiphile environment.

The extraordinary propensities of such peptide amphiphiles to form morphologies with tunable features has been utilized in the development of novel materials. Examples are tunable hydrogels, the development of delivery platforms, and as peptide amphiphiles scaffolds for regenerative medicine.[26, 36] Also, electrospinning of peptide amphiphiles as a protective layer for metal surfaces was reported to produce biocompatible coatings for medical devices.[37]

To obtain colloidally stable GNPs for a variety of (biomedical) applications, a protective coating is required. The present work aims to design peptide amphiphiles suitable for functionalization of GNPs and preventing their aggregation in a biological environment. For this, a thiol-group was introduced at the alkyl chain terminus to yield functional peptide amphiphiles generally described as mercaptoacyl-$[VA]_3K_3$, where either a mercaptohexadecanoyl or mercaptoundecanoyl chain is conjugated to a $[VA]_3$ peptide segment, representing four different peptide sequences: VVVAAA, AAAVVV, VAVAVA, and AVAVAV. In addition, thiolated peptide amphiphiles were oxidized to form dimerized peptide amphiphiles with two alkyl chains and two identical peptide domains coupled through an S-S bridge. Altering the hydrophobic segment in a peptide amphiphile may induce changes to its self-assembly behavior. Therefore, the effect of alkyl chain thiolation on the peptide amphiphile secondary structure was investigated in detail. The propensities of both thiolated and conventional amphiphiles to form ordered secondary structures and to self-assemble into supramolecular fibers were evaluated with circular dichroism (CD) and attenuated total reflection infrared spectroscopy (ATR-IR), as well as transmission electron microscopy (TEM). This approach allowed for identification of peptide amphiphiles that exhibit peptide-driven self-assembly which should be able to stabilize GNPs.

2.3 Results and Discussion

2.3.1 Peptide amphiphile design

The composition of the peptide and alkyl chain segments of the peptide amphiphiles were altered in order to tune the physical and chemical properties as well as the self-assembly behavior. For this, five different peptide domains and five alkyl chains (including two dimerized variants) were investigated (**Scheme 2.2**). The peptide amphiphiles were synthesized using solid-phase peptide synthesis according to standard Fmoc-chemistry protocols. Alkyl chains were coupled directly to the N-terminus of the peptide segment. After cleavage, the peptide amphiphiles were purified using high performance liquid chromatography (HPLC) and purity was determined by mass-spectrometry (MS, see **Figures S2.1-S2.15**). Dimerization of the thiolated peptide amphiphiles was achieved through oxidation with I_2 (**Figures S2.16-2.25**).

Peptide sequences investigated in this study contained the non-polar residues valine (Val, V) and alanine (Ala, A) in combination with the positively-charged residue lysine (Lys, K). All peptide sequences had a C-terminal amide followed by three Lys residues. Three Val and three Ala residues were either put in blocks ($\mathbf{V_3A_3}$ and $\mathbf{A_3V_3}$ in **Scheme 2.2**) or in an alternating sequence ($\mathbf{(VA)_3}$ and $\mathbf{(AV)_3}$). Also, a peptide comprising six Ala residues was synthesized ($\mathbf{A_6}$) for comparison. These sequences had either Val or Ala at the N-terminus, which was previously shown to have an effect on self-assembly propensities, as the hydrogen bond alignment is determined by the residues next to the hydrophobic core.[18]

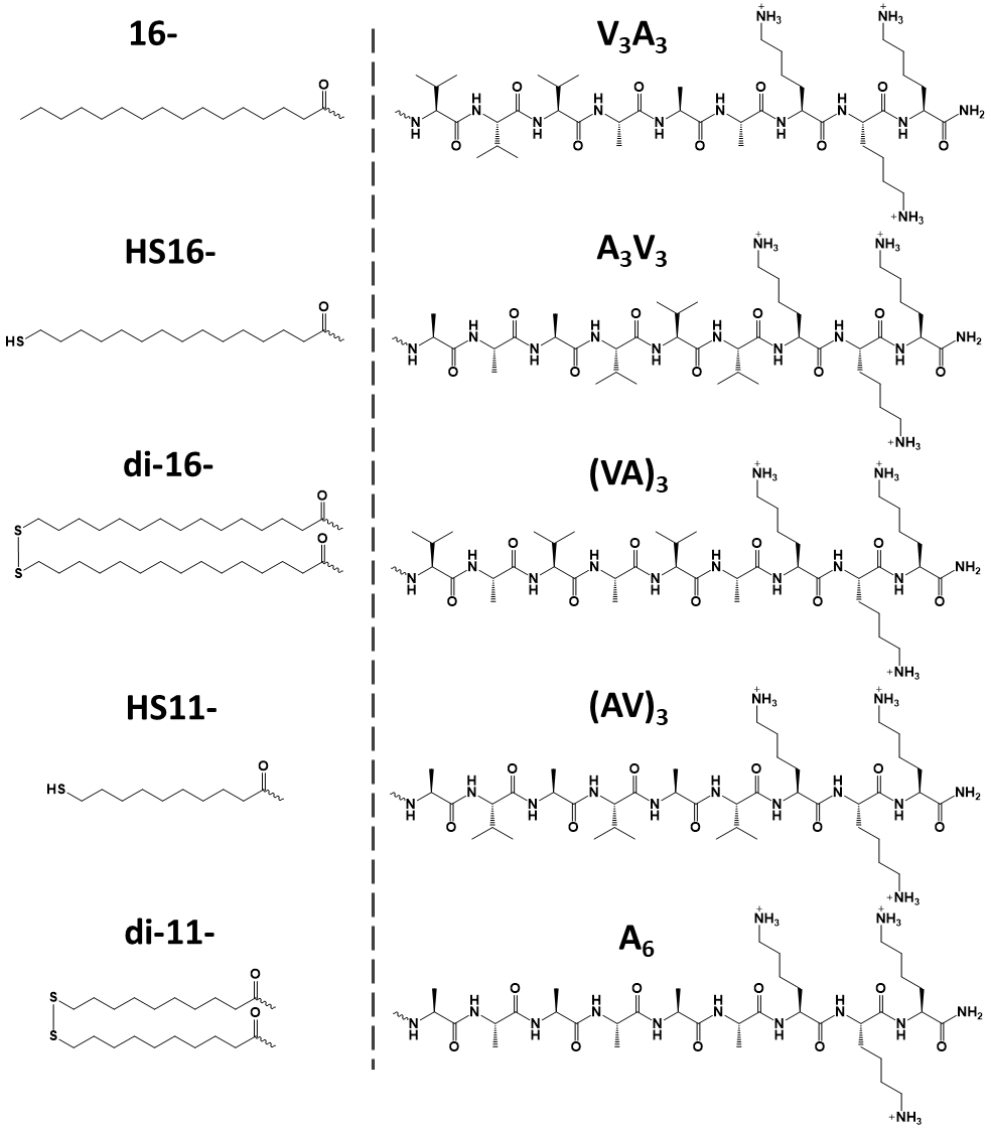

Scheme 2.2. Peptide amphiphiles were generated as a combination of one of the acyl chain options and one of the peptide sequences resulting in 25 different peptide amphiphiles. **Di-16-** and **di-11-** peptide amphiphiles comprised two identical molecules dimerized *via* the thiols to form a disulfide.

We also varied the alkyl chain length between 11 and 16 carbons. The C16 (palmitoyl) chain is typically used in peptide amphiphile designs as it was

presumed to result in more stable assemblies in comparison to shorter alkyl chains.[15, 38] Also, the resulting assembly shape may vary: cylindrical fibers were observed in the case of longer alkyl chains and micelles with shorter alkyl chains. Introduction of a thiol at the alkyl chain terminus may not only influence molecules-surface interactions but also the peptide amphiphile self-assembly process *via* dimerization. To probe the nature of the self-assembly (peptide-driven or alkyl chain-driven), peptide amphiphiles with a thiolated C11 (undecanoyl) chain were also studied, since this chain is at the lower limit of reported peptide amphiphile assemblies due to the reduced hydrophobicity.[23, 39] Palmitoylated amphiphiles were denoted as **16-** and thiolated amphiphiles were denoted as **HS16-** and **HS11-** (**Scheme 2.2**).

Oxidation of the terminal thiols was observed during storage of the peptide amphiphiles; both lyophilized and in solution (**Figure S2.26**). Close proximity of the thiols inside the fiber core most likely enabled dimer formation. It was speculated that this could change the mutual orientation of two neighboring peptide amphiphiles, giving rise to self-assembled structures with morphologies different to those formed by the monomeric species. Therefore, disulfide-bonded molecules were synthesized and evaluated as well (**di-16-** and **di-11-** in **Scheme 2.2**).

A total of 25 peptide amphiphiles were studied in this chapter. Pure peptide amphiphiles were first investigated for their propensities to form ordered peptide secondary structures using circular dichroism (CD) spectroscopy. The peptide conformation was also probed by Fourier-transform infrared spectroscopy (FT-IR) and the resulting assemblies were visualized with transmission electron microscopy (TEM).

2.3.2 Self-assembly of thiolated peptide amphiphiles

Formation of supramolecular structures can be affected by several factors, including the concentration of the self-assembling molecules and the composition of the solvent.[31, 32, 35] Circular dichroism (CD) spectroscopy is well-suited to screen peptide amphiphiles secondary structure of proteins and peptides in solution.[18, 40, 41]

The optimal concentration of peptide amphiphiles for reliable CD measurements was determined by recording spectra of **16-V_3A_3** and **HS11-V_3A_3** at different concentrations (**Figure 2.1A,B**). The spectra are typical for β-structured peptides. These peptides typically possess a minimum at 216 nm, and a maximum at 195 nm,[18, 42] but for peptide amphiphiles the minimum can be significantly red-shifted (up to 10 nm) due to a change in the mutual orientation of the peptide backbones.[18] Both peptide amphiphiles showed a minimum between 220 and 224 nm. **16-V_3A_3** showed highly comparable CD spectra in the range of 100 to 25 µM with a significant decrease in the quality of the signal at 10 µM (**Figure 2.1A**). Thus, a concentration of 50 µM was chosen for all peptide amphiphiles coupled with **16-**, and **HS16-** alkyl chains, and 25 µM for **di-16-** peptide amphiphiles. A higher optimal concentration was expected for the shorter C11 chain. **HS11-V_3A_3** at 1 mM concentration showed a significant difference in the normalized CD intensity compared to lower concentrations, suggesting that in this concentration range the linear dependence is lost (**Figure 2.1B**).[15] At 100 µM, a very low intensity was recorded, therefore, a concentration of 250 µM was chosen for all **HS11-** peptide amphiphiles, and 125 µM for **di-11-** peptide amphiphiles.

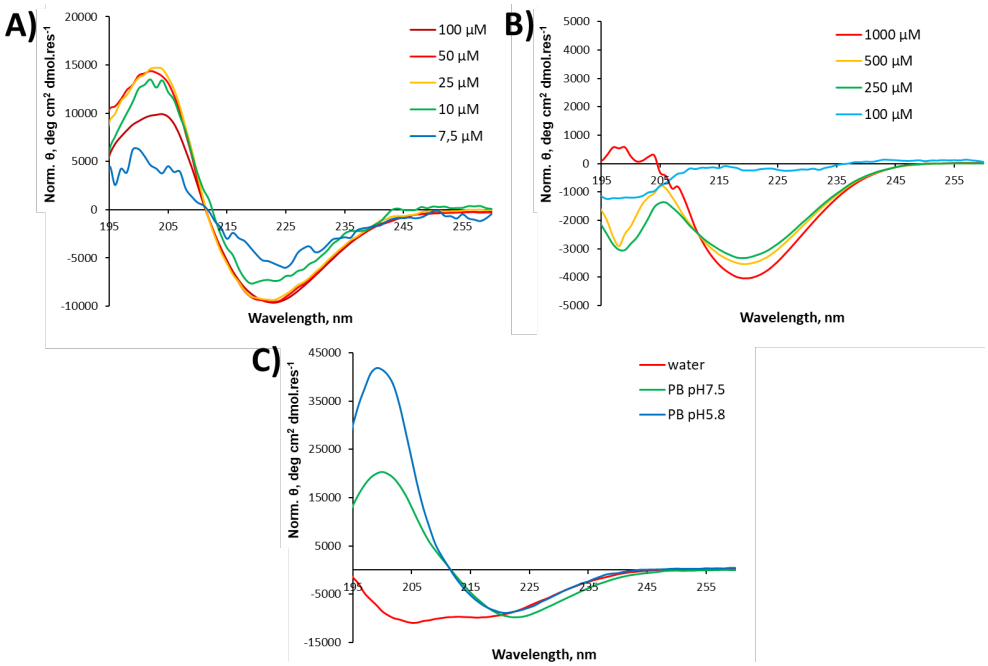

Figure 2.1. Optimization of different conditions for self-assembly monitored with CD spectroscopy: (A) **16-V$_3$A$_3$** in the concentration range of 7.5 to 100 µM (aq.); (B) **HS11-V$_3$A$_3$** in the concentration range of 100 to 1000 µM (aq.); (C) **16-(AV)$_3$** prepared in different buffers at a concentration of 100 µM. Ellipticity (θ, deg) was normalized for concentration and number of amino acid residues.

The effect of ionic strength on the secondary structure was subsequently investigated. **16-(AV)$_3$** was dissolved in water or in 10 mM phosphate buffer (PB) at two different pHs: 5.8 and 7.5 (**Figure 2.1C**). In all cases the peptide amphiphiles had protonated lysine side chains. Significant differences were observed: **16-(AV)$_3$** prepared in water showed a noticeable presence of α-helical structures (minima at 206 nm and 220 nm), at pH 7.5 the minimum at 223 nm was attributed to β-structures, also a small shoulder at 210 nm was observed. In PB at pH 5.8 the peptide amphiphile was predominantly β-structured, indicated by a single minimum at 221 nm. Interestingly, at pH 7.5 the maximum was red-shifted and broad, indicating less-ordered structures when compared to the peptide amphiphile at pH 5.8. In the remaining

chapter, samples were therefore analyzed in PB at pH 5.8, although published reports on **16-V_3A_3** utilized neutral pH conditions for assessment of the self-assembly properties.[43]

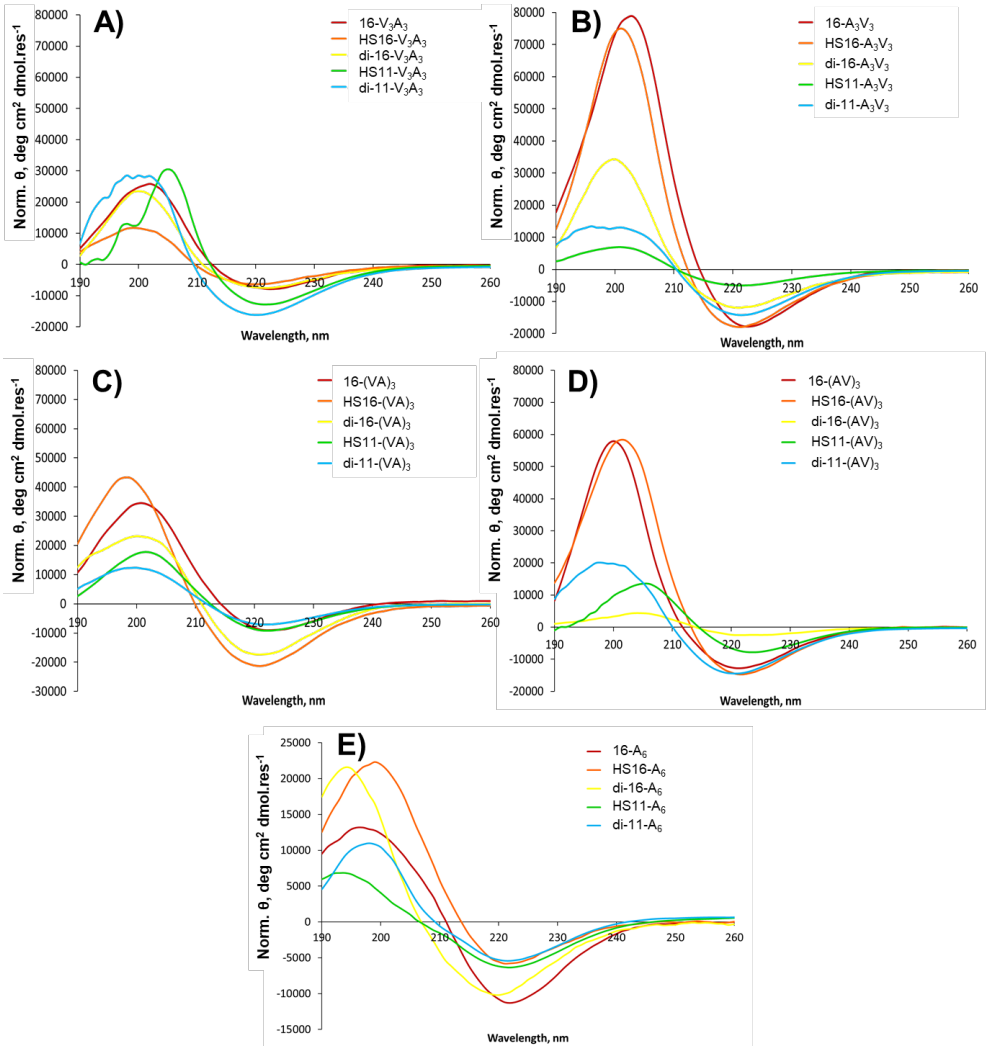

Figure 2.2. CD spectra for peptide amphiphiles: (A) **V_3A_3**; (B) **A_3V_3**; (C) **$(VA)_3$;** (D) **$(AV)_3$**; (E) **A_6**. Samples were prepared in 10 mM PB (pH 5.8).

Next, the self-assembly of all 25 synthesized peptide amphiphiles was probed with CD spectroscopy (**Figure 2.2**). Only peptide amphiphiles with the $\mathbf{A_6}$ domain deviated from the typical β-structure (**Figure 2.2**). The minimum position and peak intensity of **HS16-** peptide amphiphiles were compared to their **C16-** counterparts to obtain insight in the hydrogen bond alignment and β-structure-forming ability.[18]

The $\mathbf{V_3A_3}$ domain did not undergo a significant rearrangement when the **16-** chain was replaced by **di-16-**, only a slight blue-shift (-2 nm) in the minimum position was observed for **HS16-$\mathbf{V_3A_3}$** (**Figure 2.2A**). Shortening the alkyl chain to **HS11-** caused a higher molar ellipticity, while dimerization resulted in peak broadening. The reversed block sequence, $\mathbf{A_3V_3}$, responded to the alkyl chain alteration differently (**Figure 2.2B**): thiolation of the C16 chain resulted in a blue-shift and dimerization to **di-16-$\mathbf{A_3V_3}$** significantly reduced the peak minimum intensity. Shortening the alkyl chain reduced the peak intensity by almost 25%, but dimerization of **HS11-$\mathbf{A_3V_3}$** restored the signal to the level of **di-16-$\mathbf{A_3V_3}$**.

Interestingly, thiolation of **16-$\mathbf{(VA)_3}$** significantly enhanced the CD signal, and the dimerized **di-16-$\mathbf{(VA)_3}$** showed almost the same minimum intensity (**Figure 2.2C**). Almost no difference in the minimum intensity was detected between **16-$\mathbf{(VA)_3}$**, **HS11-$\mathbf{(VA)_3}$**, and **di-11-$\mathbf{(VA)_3}$**, yet peak broadening was apparent for the two thiolated amphiphiles. The second alternating peptide domain **$\mathbf{(AV)_3}$** (**Figure 2.2D**) responded to thiolation in a similar fashion as $\mathbf{A_3V_3}$: **16-** and **HS16-** variants showed minimal differences, while **di-16-** was again less structured. In summary, $\mathbf{A_3V_3}$ and **$\mathbf{(AV)_3}$** behaved quite comparable. Interestingly, the similarities between the two peptide domains were maintained for the **HS11-** and **di-11-** coupled molecules: the intensity of the **HS11-$\mathbf{(AV)_3}$** spectrum was significantly lower compared to **di-11-$\mathbf{(AV)_3}$**.

Also, **HS11-$(AV)_3$** showed the highest red-shift (+3 nm) relative to its **16-** variant. These differences imply a significant rearrangement within the assemblies.

A_6 peptide amphiphiles revealed the lowest overall ellipticity signal for all five variants (**Figure 2.2E**). Thiolation of the C16 chain led to a significant reduction of the signal for **HS16-A_6**. Shortening the thiolated chain to **HS11-A_6** resulted in a CD spectrum that could not belong to a predominantly β-structured peptide amphiphile. A shoulder at 208 nm could either be explained by a blue-shift of the minimum position or a contribution from an α-helical structure.[41] Similar small shoulders were evident for the dimerized molecules **di-16-A_6** and **di-11-A_6**.

In summary, while some similarities and trends between peptide domains could be observed, especially for the **A_3V_3** and **$(AV)_3$** domains, it was clear that both the peptide and alkyl chain domains affected the peptide amphiphile self-assembly behavior.

Thiols are prone to oxidation, as after prolonged storage (>3 months, RT, both solid state and in solution) the formation of dimers was observed with LC-MS (**Figure S2.26**). Two reducing agents, tris(2-carboxyethyl)phosphine (TCEP) or dithiothreitol (DTT), were therefore tested for their ability to prevent oxidation. TCEP or DTT (2 eq.) was added to the solvent (water) prior to dissolution of a peptide amphiphile and the peptide amphiphile self-assembly was monitored with CD spectroscopy (**Figure 2.3**). Surprisingly, TCEP disturbed the self-assembly of both **16-V_3A_3** and **HS16-V_3A_3** amphiphiles. With respect to an aqueous or buffered solution, TCEP addition to **16-V_3A_3** resulted in a significant increase of molar ellipticity indicative of more intense polarized light scattering by the assemblies and hence a

different mode of self-assembly (**Figure 2.3A**).[18] However, TCEP addition to a **HS16-V_3A_3** solution prompted formation of significantly less ordered assemblies (**Figure 2.3B**). DTT seemed to have a milder effect on the thiolated peptide amphiphiles as CD spectra of **HS16-V_3A_3** prepared in the presence and absence of DTT were identical. However, that was not the case for all thiolated peptide amphiphiles. Therefore, it was decided not to use any reducing agents in the remainder of this study.

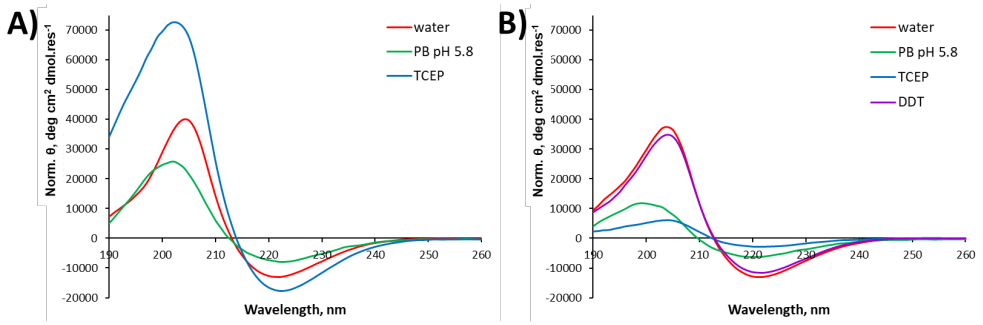

Figure 2.3. The effect of reducing agents on peptide amphiphile self-assembly monitored with CD spectroscopy: (A) **16-V_3A_3** prepared at a concentration of 100 μM with and without reducing agents; and (B) **HS16-V_3A_3** prepared at a concentration of 100 μM with and without reducing agents.

To obtain insight into the β-content within the assemblies, attenuated total reflection Fourier-transform infra-red spectroscopy (ATR-FTIR) spectra of lyophilized peptide amphiphiles were recorded (**Figure 2.4** and **Figure S2.27-S2.31**). The Amide I peak is typically centered between 1575-1725 cm^{-1} and represents a superposition of signals deriving from different conformations of the peptide backbone: 1627-1640 cm^{-1} is attributed to β-structures; 1647-1654 cm^{-1} to α-structures; and 1650-1670 cm^{-1} to random and other structures.[44, 45]

The Amide I peak overlaps with peaks corresponding to the C-terminal amide (around 1615 cm^{-1}) and the Lys side chain amine (1629 cm^{-1}). Therefore, the

Amide I peak was fitted to three peaks with maxima at 1615 cm^{-1}, 1630 cm^{-1}, and 1667 cm^{-1} (**Figure 2.4A**). These positions were present in all spectra, although small shifts occurred for some of the samples (**Figure S2.27-S2.31**). If a peak at 1654 cm^{-1}, indicative of α-structure, could be resolved, it was added to the fitting procedure. IR spectra of lysine-containing peptides are known to be sensitive to the pH of the solution they are lyophilized from, resulting in a peak shift and peak broadening.[46, 47] The two bands centered at 1615 cm^{-1} and 1630 cm^{-1} overlap in a way that does not allow for good-resolution fitting. Therefore, the joint contribution of β-structures and primary amines of lysine side chains was compared. This value was considered to reflect the content of β-structures in the samples, while the rest of the Amide I peak was attributed to other structures. The β-associated content for all 25 peptide amphiphiles is summarized in a heatmap (**Figure 2.4B**).

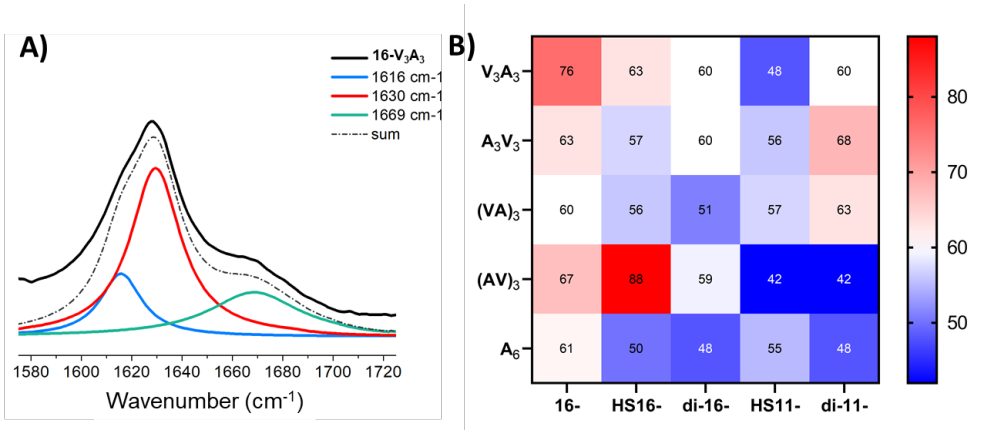

Figure 2.4. Characterization of self-assembly behavior by means of ATR-IR spectroscopy: (A) Amide I peak fitting for **16-V_3A_3** and (B) a heatmap illustrating the β-associated content derived from the Amide I peak fitting, blue shades represent low amounts of β-structure whereas red shades indicate a high percentage of β-structure. Near-white shades indicate an average level of β-structure for these systems.

Interestingly, it was only possible to resolve a peak at 1654 cm^{-1} for some of the thiolated peptide amphiphiles, and it was absent in all palmitoylated peptide amphiphiles (**Figure S2.27-S2.31**). Relatively low levels of self-assembly (β-associated content < 60% and high α-content – between 10 and 25%) were observed for the $\mathbf{A_6}$ amphiphiles, which is in good agreement with the CD data (**Figure 2.2E**, **Figure S2.31**). For the $\mathbf{V_3A_3}$ peptide domain (**Figure S2.27**) thiolation of the C16 alkyl chain had a negative effect: the β-content dropped from 76% to 63%. Dimerization of the latter molecule did not significantly change the structure of the peptide domain, consistent with the CD spectra. **HS11-$\mathbf{V_3A_3}$** showed 48% β-content, but its dimer **di-11-$\mathbf{V_3A_3}$** was comparable to more structured C16 peptide amphiphiles. The $\mathbf{A_3V_3}$ peptide domain showed a smaller change when the alkyl chain composition was altered: the β-associated content ranged between 56 and 68% (**Figure S2.27**) with **di-11-$\mathbf{A_3V_3}$** being the most β-structured. On the other hand, alternating sequences $\mathbf{(VA)_3}$ and $\mathbf{(AV)_3}$ showed more deviant behavior. In general, **16-$\mathbf{(VA)_3}$** showed the lowest β-associated content (60%) among all palmitoylated peptide amphiphiles (**Figure S2.29**). Although thiolation or shortening the alkyl chain to yield **HS16-** and **HS11-** variants did not significantly change the β-associated content, dimerization of these molecules showed an opposite effect. One particular feature was observed for the $\mathbf{(AV)_3}$ peptide domain: it was the only example where thiolation of the C16 chain gave rise to a more β-structured assembly (67 *versus* 88%, **Figure S2.30**). All other variants (**di-16-**, **HS11-**, **di-11-**) showed a β-associated content below 60%. **HS11-$\mathbf{(AV)_3}$** and **di-11-$\mathbf{(AV)_3}$** also contained α-structures. In some instances, results of the CD analysis would signify a certain value for the β-associated content, but these trends were not necessarily observed with FTIR analysis. For example, the CD spectra of **16-$\mathbf{(VA)_3}$** and **HS16-$\mathbf{(VA)_3}$** would suggest a higher level of self-assembly for the

latter, but according to the FTIR data, the β-associated content did not significantly differ between the two (**Figure 2.2C** and **Figure 2.4B**). In contrast, the **16-$(AV)_3$** and **HS16-$(AV)_3$** had similar CD spectra, however FTIR showed the latter was significantly more β-structured (**Figure 2.2D** and **Figure 2.4B**).

In summary, the combined CD and FT-IR study on the secondary structure of each peptide domain revealed that finding common self-assembly trends is not trivial. In general, thiolated peptide amphiphiles were less structured than their C16 counterparts. Dimerization and substitution of the C16 alkyl chain for C11 had different impacts depending on the peptide sequence. The discrepancies between the CD and IR spectra observed for some samples, could be attributed to the differences in preparation method, and also to the concentration of the samples, which has already been established to affect the amphiphile self-assembly (see **Figure 2.1**).

To obtain more insight on the effect of thiolation and dimerization of peptide amphiphiles on self-assembly in solution, transmission electron microscopy (TEM) imaging was performed.

2.3.3 Evaluation of peptide amphiphile fibers in TEM

For TEM analysis, samples were prepared in 10 mM PB (pH 5.8) and aged for 14 days, deposited on carbon TEM grids and negatively stained with 0.5% uranyl acetate (**Figure 2.5**). All peptide amphiphiles assembled into cylindrical fibers as was previously reported for palmitoyl (C16) peptide amphiphiles.[28] This indicated that thiolation did not disrupt self-assembly, or affect fiber morphology, thus maintaining the fiber core sequestered from the aqueous environment due to effective hydrophobic collapse. Since images were acquired relatively close to focus with a certain defocus needed, and

most of the samples were represented as fiber bundles, quantitative information based on the TEM images, such as true fiber thickness, could not be obtained. Nonetheless, all observed fibers had a diameter of ~9 nm, corresponding to the length of two peptide amphiphiles, irrespective of the peptide domain composition.[33]

Fibers composed of palmitoyl peptide amphiphiles were very long (typically >500 nm) and aligned into sheets (top panels in **Figure 2.5)**. Also, some sort of fracturing of these stacks appeared to be present in some images, *e.g.* see **16-(AV)$_3$**. Sample preparation could have caused these effects, since the samples were blotted and dried on the TEM grid, but it was not possible to determine the exact reason for fracturing.[48] It was obvious that thiol introduction reduced the average fiber length irrespective of peptide domain composition. Furthermore, all five dimeric (**di-16-**) peptide amphiphiles formed very short fibers (<200 nm). In contrast, no general trend was observed for **HS11-** peptide amphiphiles: **HS11-V$_3$A$_3$**, **HS11-A$_3$V$_3$**, or **HS11-(VA)$_3$** showed a similar length distribution as their **HS16-** counterparts, while intense bundling was observed for **HS11-(AV)$_3$** or no fiber interaction at all (**HS11-A$_6$**). No clear tendency was observed that would unify the effect of thiolation on fiber formation. Dimerization of C11 peptide amphiphiles changed the appearance of the fibers (except for **di-11-V$_3$A$_3$**): it either made the assemblies more defined and long, similar to their **16-** counterparts (**di-11-A$_6$**); reduced the interaction between individual fibers (**di-11-(VA)$_3$**); or on the contrary, induced more fiber bundling (**di-11-A$_3$V$_3$** and **di-11-(AV)$_3$**). Due to the variety of formed assemblies, it appeared that the self-assembly of C11 peptide amphiphiles was more sensitive towards the peptide sequence as compared to their C16 variants. Most of the **HS11-** peptide amphiphiles showed less β-associated content and/or significant contributions of α- and other structures. Moreover, dimers of thiolated peptide amphiphiles like **di-**

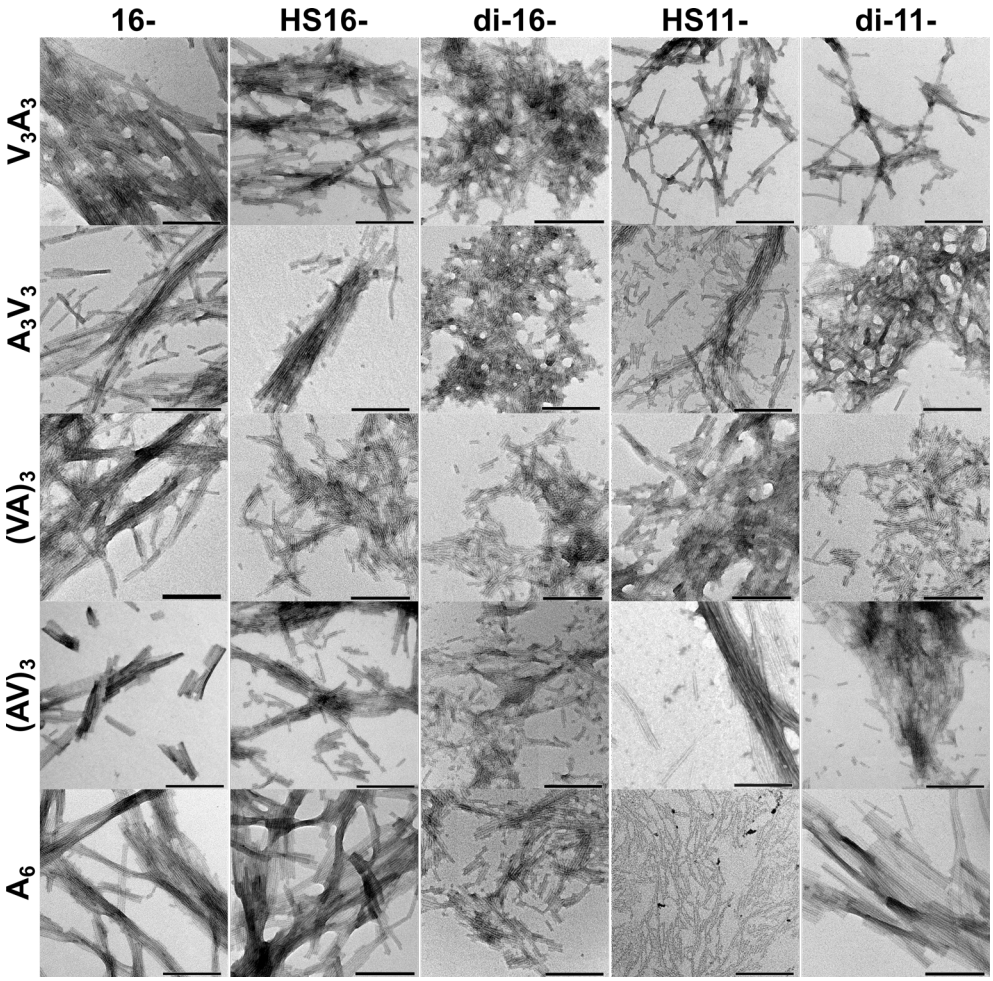

Figure 2.5. Representative TEM images of peptide amphiphiles (uranyl acetate stained). Columns show evolution of the same peptide domain conjugated to different alkyl chains, while rows show evolution of the same alkyl chain conjugated to different peptide portions. Samples were prepared in 10 mM PB (pH 5.8) at peptide amphiphile concentrations of: 50 μM for **16-** and **HS16-** samples; 25 μM for **di-16-**; 250 μM for **HS11-**; and 125 μM for **di-11-**. Scale bar is 200 nm.

16-A_3V_3 and **di-11-A_3V_3** formed almost 3D-like morphologies with pore-like patterns formed by fiber bundling. Notably, dimers showed better length distributions and intensive bundling. A clear difference between **V_3A_3**, or **$(VA)_3$**, and **A_3V_3**, **$(AV)_3$**, or **A_6** was observed: the latter amphiphiles tended to

form rope-like fiber bundles, stacks covering vast areas, while the former amphiphiles yielded smaller-scale structures. Thiolated variants of **A_6** peptide amphiphiles distinctly differed from the rest of the samples, which was attributed to the low β-content and high α-content (**Figure 2.4B**).

In summary, TEM imaging revealed large differences in fiber appearance between palmitoyl and thiolated peptide amphiphiles. Additionally, the difference between fibers formed by highly β-structured molecules (such as all **16-** samples) and molecules with high α-content (for example, **HS11-A_6** – 25% α-structures) was observed. Peptide amphiphiles coupled to the **V_3A_3** peptide headgroup were arguably the only tested group that exhibited relatively similar fiber appearance for all five alkyl chain variants.

2.3.4 Analysis of fiber formation

Through the combined use of CD, FTIR, and TEM, the secondary structure and self-assembly properties of 25 different peptide amphiphiles was assessed. The data obtained supports the hypothesis that the geometry of the molecule, in addition to its composition, defines its self-assembly behavior.

A more in-depth CD analysis can unravel how peptide amphiphile molecules are orientated within the fibers.[18] The minimum position characterizes the internal orientation of peptide chains. If peptide backbones form flat stacks that propagate along the fiber axis (**Scheme 2.3**, upper panel), the peptide amphiphile will have a CD minimum at ~216 nm.[18] But if the aligned peptide backbones propagate in twisted spirals (**Scheme 2.3**, lower panel), then the minimum will be red-shifted proportional to the amount of twisting. It was shown that the internal twisting was affected by the number of valine and alanine residues, as well as their position in the peptide segment. In

comparison to palmitoyl-$V_4A_2E_3$, palmitoyl-$A_3V_3E_3$ showed more intense internal twisting within the fibers associated with concomitant changes in hydrogen bond alignment and assemblies stability.[18, 28] It was therefore anticipated that by varying the alkyl chain composition, the propensities to form intermolecular hydrogen bonds, and hence β-structures, could be affected too.

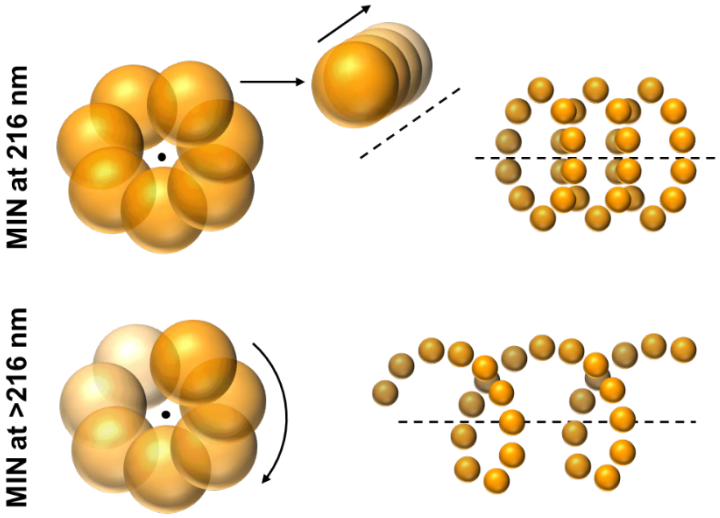

Scheme 2.3. CD minimum position defines the propagation mode of molecules within a supramolecular fiber. Spheres represent individual peptide amphiphiles. Peptide amphiphile backbones are perpendicular to the fiber propagation axis (dashed line). When molecules propagate as flat stacks along the fiber axis, then the ellipticity minimum is typically located at 216 nm. When molecules propagate along the fiber axis with a twist, a red-shift of the ellipticity minimum is observed.[18]

To investigate the internal organization of the fibers, the ellipticity minima (θ_{min}) were compared (**Figure 2.6B**, top graph). The average value for the minimum position amongst the 25 studied peptide amphiphiles was at 221 nm. The intensity of the peak centered around 221 nm is dependent on the order within the assemblies (**Figure 2.6B**, bottom graph). Peptide amphiphile assemblies scatter circularly polarized light.[18] For example, intense fiber bundling causes more light scattering, and hence, an increase

in the θ_{min} intensity. However, since the CD signal is a superposition of different secondary structures, contributions of which can also affect the θ_{min} intensity in the predominantly β-structured assemblies. Thus, the θ intensity at 221 nm (θ_{221}) is a measure of β-structures contribution. Furthermore, assemblies with more internal twisting would have larger hydrogen-bonding distances, which potentially introduce packing defects such as the presence of unordered structures and cause the θ_{min} intensity to change.

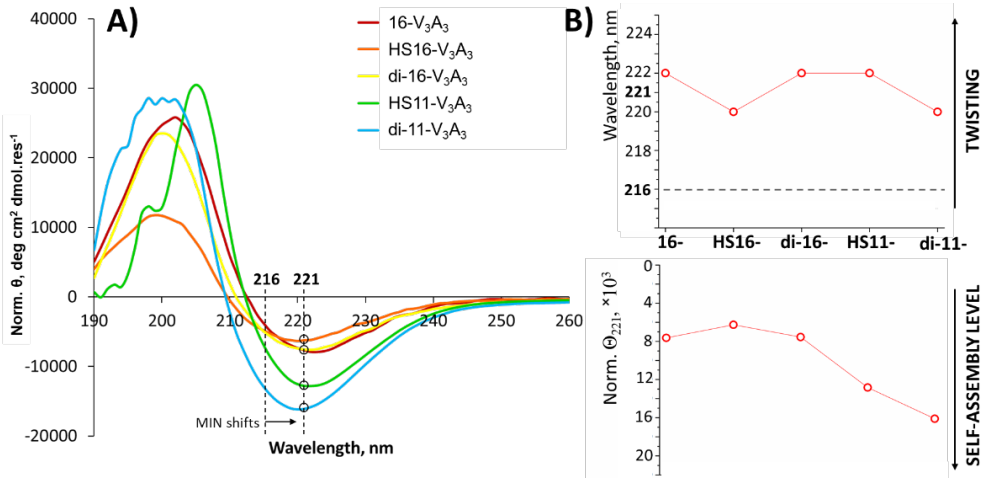

Figure 2.6. Characterization of self-assembly behavior using CD spectroscopy: (A) CD spectra for all **V_3A_3** peptide amphiphiles; (B) minimum positions (top panel) and normalized ellipticity minimum (bottom panel). Samples were prepared in 10 mM PB (pH 5.8).

The same approach was applied to the other peptide amphiphiles (**Figure 2.7**). With respect to their C16 variants, the θ_{min} did not significantly shift for thiolated peptide amphiphiles with a **A_3V_3** and **$(VA)_3$** domain. **$(AV)_3$** and **A_6** peptide amphiphiles showed ±1-3 nm θ_{min} shifts indicative of notable hydrogen bond rearrangement within the fibers. In terms of θ_{min} position and internal twisting, with respect to the average, only **HS11-$(AV)_3$** showed more

internal twisting, while **HS16-A_3V_3** and **HS11-A_6** showed less, but the β-content decreased for all three peptide amphiphiles. Interestingly, more intense internal twisting was associated with a stronger impact on the β-content than less internal twisting: - 25% for **HS11-$(AV)_3$** *versus* -13% for **HS16-A_3V_3** and **HS11-A_6**. As **HS11-$(AV)_3$** showed a significant increase in α-content, it seems as if more internal twisting weakened intramolecular hydrogen bonding, but allowed for more effective intermolecular hydrogen bonding. Interestingly, a common trend was observed for **16-** variants compared to **HS16-** variants for all peptide domains except **$(AV)_3$**: the θ_{min} position was less shifted from 216 nm, hence, less internal twisting was expected, but the β-associated content decreased. Notably, **HS16-** fibers were shorter than their **16-** analogues (**Figure 2.5**). **HS16-$(VA)_3$** showed the most intense CD spectrum when compared to **16-$(VA)_3$**, suggestive of a more-ordered structure.

Dimerization of **HS16-** peptide amphiphiles did not significantly affect the β-associated content (from -5 to +3%), except for the **$(AV)_3$** domain (**Figure 2.4**). Importantly, the β-associated content for all **di-16-** peptide amphiphiles was within the 48-60% range. Also, the least β-structured **A_6** domain was not dramatically affected by dimerization. Unlike the **HS16-** peptide amphiphiles, all **di-16-** fibers showed similar fiber bundling (**Figure 2.5**).

Furthermore, **HS11-** peptide amphiphiles were compared to their **16-** counterparts. All **HS11-** peptide amphiphiles were less β-structured and assembled into shorter fibers (**Figure 2.5** and **Figure 2.7**). When compared to the **HS16-** analogues, **HS11-** demonstrates moderate β-associated content values: 42-57% *versus* 50-88%. Also, broadening of the FT-IR

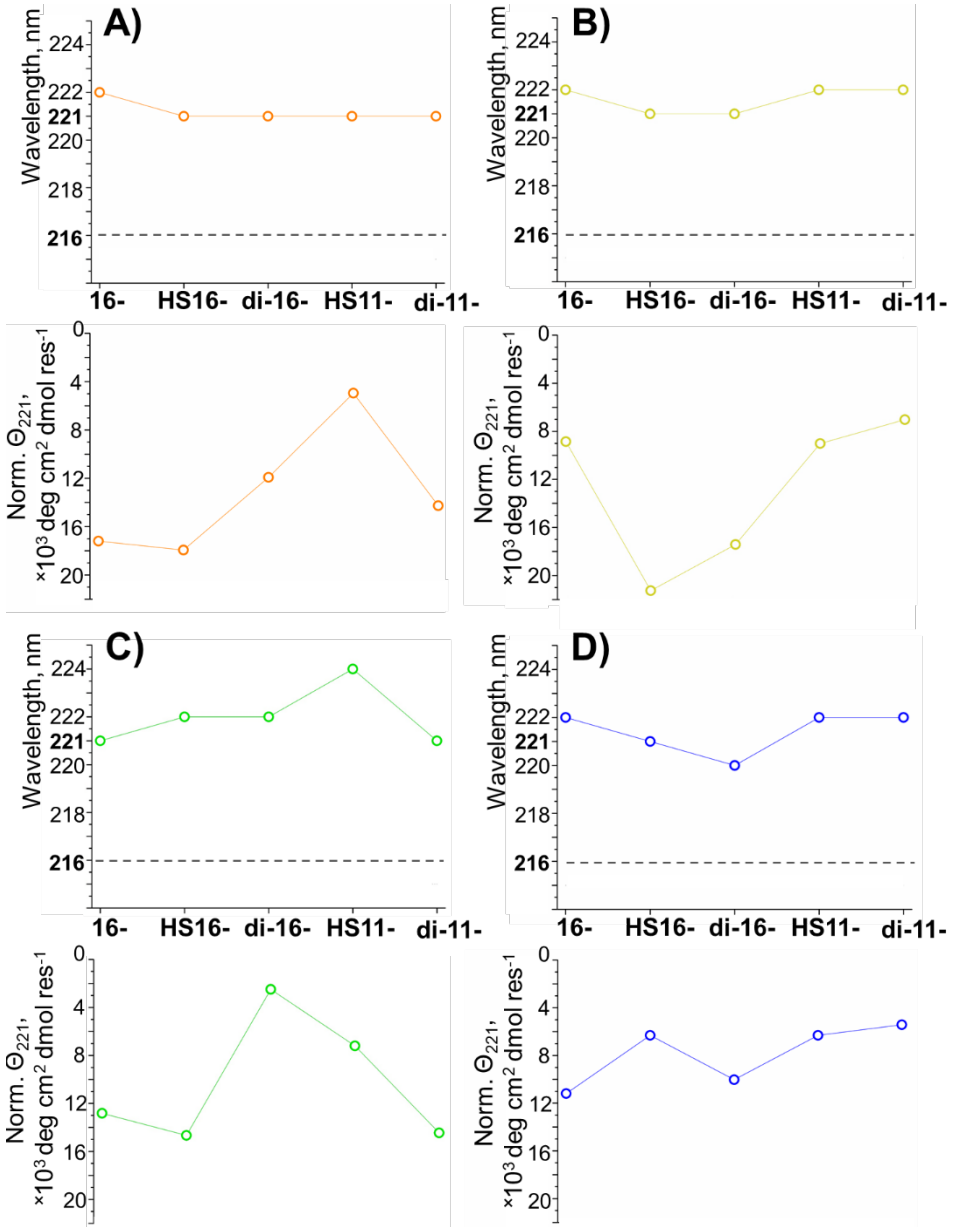

Figure 2.7. Characterization of self-assembly behavior using CD spectroscopy for different peptide amphiphiles: (A) $\mathbf{A_3V_3}$; (B) $\mathbf{(VA)_3}$; (C) $\mathbf{(AV)_3}$; and (D) $\mathbf{A_6}$. Samples were prepared in 10 mM PB (pH 5.8).

absorption band centered around 1630 cm^{-1} typical for **HS11-** peptide amphiphiles indicated an increased contribution of α-structures in comparison to the C16 variants (especially, $\mathbf{V_3A_3}$ and $\mathbf{(AV)_3}$). However, it was not possible to link a change in the θ_{min} position with a one-directional change in the level of self-assembly when **HS16-** analogues were compared to their **HS11-** variants.

The dimers **di-11-$\mathbf{A_3V_3}$** and **di-11-$\mathbf{(VA)_3}$** have the same degree of internal twisting as their monomeric counterparts, but a higher level of self-assembly and β-associated content, as well as θ_{min} intensity. Also, fiber formation in the case of **di11-$\mathbf{V_3A_3}$** and **di11-$\mathbf{A_3V_3}$** was similar to their monomeric species. This was not the case for **di11-$\mathbf{(VA)_3}$**, **di11-$\mathbf{(AV)_3}$**, and **di11-$_6$**. **Di-11-$\mathbf{A_6}$**: while the mutual orientation of peptide amphiphiles within the fibers did not change with respect to **HS11-$\mathbf{A_6}$**, the β-associated content decreased due to an increase in contributions coming from other secondary structures (1672 cm^{-1}). Interestingly, fibers formed by **di-11-$\mathbf{A_6}$** appeared to be more defined and formed one-layer stacks, while **HS11-$\mathbf{A_6}$** fibers showed a deviant thickness and no integration into a network (**Figure 2.5**), probably due to the presence of α-helices (**Figure S2.31**). This behavior was also observed for **HS11-$\mathbf{(AV)_3}$** versus **di11-$\mathbf{(AV)_3}$.** Interestingly, peptide amphiphiles with $\mathbf{V_3A_3}$ and $\mathbf{(VA)_3}$ domains showed less variations in terms of their β-associated content than $\mathbf{A_6}$-, $\mathbf{A_3V_3}$-, and $\mathbf{(AV)_3}$-based peptide amphiphiles. This suggests that the first Val residue next to the hydrophobic core, is important in terms of hydrogen bond alignment. No clear common trends for $\mathbf{V_3A_3}$ and $\mathbf{(VA)_3}$ or $\mathbf{A_6}$, $\mathbf{A_3V_3}$, and $\mathbf{(AV)_3}$ could be established however. Nevertheless, it shows that the molecule geometry plays an important role: block sequences $\mathbf{V_3A_3}$ and $\mathbf{A_3V_3}$ were more structured and less responsive to alterations in the alkyl chain composition, as compared to alternating sequences $\mathbf{(VA)_3}$ or $\mathbf{(AV)_3}$. No hydrogen bond rearrangements occurred upon changing the alkyl chain

length for the **A_3V_3** peptide amphiphiles (**Figure 2.2B,D**). Hydrogen bond alignment within **$(AV)_3$** peptide amphiphile assemblies was the most susceptible to every change in the alkyl chain. As expected, **A_6**-based amphiphiles possessed the lowest β-structure propensity among all peptide amphiphiles tested regardless of the alkyl chain properties (**Figure 2.7D**). Finally, the presence of an α-helical component was observed for all **HS11-** variants (**Figure S2.27-S2.31**).

Presumably, due to the higher hydrophobicity of Val compared to Ala and a small increase in steric bulk of the side chain, a tighter packing with less monomer freedom is possible within the supramolecular fiber. From the obtained data it is clear that the first amino acid residues (two or potentially even three) next to the alkyl chain are crucial for the resulting assembly's rigidity, which is in line with literature.[18]

Within this study it was not possible to distinguish a single parameter that would define the "best" self-assembly behavior: the θ_{min} position, determination of internal twisting within the fibers and hydrogen bond alignment, did not always directly follow the change in the β-associated content. Self-assembly is a complex process and one change in chemical composition of the monomer can induce simultaneous changes of several parameters as has been shown in this study. From the obtained data, the **V_3A_3** peptide domain appears to be the most suited for functionalization of metal surfaces. This peptide domain is robust in terms of preserving the β-content upon modifications of the alkyl chain. These findings open up the possibility of using thiolated peptide amphiphiles to form a highly ordered self-assembled monolayer (SAM) on the curved surface of gold nanoparticles.

2.4 Conclusions

The self-assembly of peptide amphiphiles is dependent on both the peptide domain and the alkyl chain used. From the structural analysis based on CD and FT-IR spectroscopy data, peptide amphiphiles could be divided into two groups based on the mode of self-assembly: peptide-driven or driven by alkyl chain characteristics. This study shows that a peptide sequence with amino acid residues arranged in blocks of three is beneficial, as the block $\mathbf{V_3A_3}$ and $\mathbf{A_3V_3}$ sequences were less responsive to changes in alkyl chain length and composition. They consistently demonstrated more-ordered self-assemblies and possessed the ability to adopt a β-strand conformation when coupled to different alkyl chains, while alternating sequences $\mathbf{(VA)_3}$ and $\mathbf{(AV)_3}$ rearranged the hydrogen bond alignment in response to every change in the alkyl chain composition. In contrast, peptide amphiphiles with alternating peptide domains ($\mathbf{(VA)_3}$ and $\mathbf{(AV)_3}$) were more sensitive to changes to the alkyl chain composition. These sequences showed dramatically different self-assembly behavior for palmitoyl and thiolated variants, as well as for monomeric and dimeric species.

Ultimately, this study provides design rules and synthetic procedures for thiolated peptide amphiphiles with a high level of self-assembly and high β-content. Depending on the composition, thiolated peptide amphiphiles can be as structured as conventional palmitoyl peptide amphiphiles, and they offer new approaches in surface modification and systems where redox reactions are of value. In the system where rigid assemblies on a surface are required, as for example, surface stabilization of GNPs, thiolated peptide amphiphiles can be used. From this perspective, the $\mathbf{V_3A_3}$ peptide domain was chosen for the further work on coating gold nanoparticles of different shape and size. **Chapters 3** and **4** of this thesis demonstrate performance of $\mathbf{V_3A_3}$-based peptide amphiphiles on the surface of gold nanoparticles of different size and shape.

2.5 Experimental section

2.5.1 Materials

All chemicals were purchased from Sigma-Aldrich except where stated otherwise. TFA, piperidine, DMF, DCM, methanol, and acetonitrile were purchased from Biosolve. Oxyma pure was supplied by Carl Roth GmbH. Formvar Carbon/Copper (200 mesh) TEM grids were purchased from Electron Microscopy Sciences.

2.5.2 Peptide amphiphile synthesis

All peptide amphiphile sequences were synthesized by solid-phase peptide synthesis using standard Fmoc-chemistry protocols (9-fluorenylmethyloxycarbonyl-protected amino acids were used to propagate the peptide chain). The synthesis was performed on an automated microwave peptide synthesizer Liberty Blue (CEM) using standard settings. 5 equivalents (relative to the resin loading) of Fmoc-protected amino acids were used to propagate the peptide chain. 20% piperidine in DMF was used as the deprotection agent (90 °C, 60 secs) and DIC/Oxyma were employed as activator/activator base (5 equivalents relative to the resin loading, 95 °C, 4 mins). All sequences were synthesized on a high-loading Rink Amide resin, which yields a C-terminal amide. The alkyl chains were introduced *via* an on-resin coupling of the corresponding chain to the terminal amine of the corresponding peptide (the same protocol as for amino acid coupling). The list of peptides and alkyl chains is shown in **Scheme 2.2.** All the molecules were cleaved from the resin using a trifluoroacetic acid (TFA) cocktail with 1.5% deionized water, 2.5% triisopropylsilane (TIS), and 2.5% 3,4-

ethylenedioxythiophene (EDOT) for thiolated peptide amphiphiles only (2 hours, RT). The crude amphiphiles were precipitated into cold diethyl ether, pelleted by centrifugation, redissolved in water, and lyophilized prior to purification.

2.5.3 Peptide amphiphile purification

HPLC purification was performed on a Shimadzu system equipped with two LC-20AR pumps, an SPD-20A UV-Vis detector and a Phenomenex Kinetex EVO C18 column. The mobile phases were water and acetonitrile, containing 0.1% TFA. The purity of the compounds was assessed using LC-MS (**Figures S2.1-S2.15**). All purified molecules were lyophilized and stored at -20 °C until required. VariPure IPE (PL3540-D603VP, 100 mg, Agilent) columns were used to capture and remove TFA traces from the sample after purification and drying if needed.

2.5.4 Peptide amphiphile dimerization

Dimerization was conducted *via* oxidation of terminal thiols with iodine to form a disulfide bridge. A peptide amphiphile was dissolved in 80% methanol at a concentration of 2 mg/mL and 0.5 M iodine solution was added dropwise to the stirred solution. The addition of iodine was stopped as soon as the color became persistently yellow. Stirring was continued for another 15 min and excess iodine was quenched with 1 M ascorbic acid. Methanol was evaporated and the presence of the dimers was confirmed with LC-MS. Dimerized amphiphiles were purified and lyophilized in the same way as described above. The purity of the compounds was assessed using LC-MS (**Figures S2.16-S2.25**).

2.5.5 Circular dichroism measurements

Circular dichroism (CD) spectra of the amphiphiles were recorded using a JASCO J-815 spectropolarimeter, fitted with a Peltier temperature controller. All measurements were performed at 20 °C. Lyophilized powders of peptide amphiphiles were dissolved in 10 mM PB (pH 5.8) at the following concentrations: 50 μM for peptide amphiphiles terminated with **16-** and **HS16-** alkyl chains; 25 μM for peptide amphiphiles terminated with **di16-** chains; 250 μM for peptide amphiphiles terminated with **HS11-** alkyl chains; and 125 μM for peptide amphiphiles terminated with **di11-** alkyl chains. Samples were left in the dark in sealed vials for 14 days to age. Samples were measured in quartz cuvettes with a 12 mm path length, and spectra were recorded from 260 to 190 nm at 1 nm intervals with a 1 nm bandwidth. All spectra were converted to mean residue ellipticity (deg cm^2 $dmol\ res^{-1}$) using equation 1:

$$[\theta] = \frac{100 * [\theta]obs}{c * n * l} \quad (1)$$

where $[\theta]_{obs}$ is the observed ellipticity in mdeg, c is the concentration of the sample in mM, n is the number of amino acids in the peptide or amphiphile and l is the path length of the cuvette in cm.

2.5.6 Infra-red spectroscopy measurements

Attenuated total reflection-infrared (ATR-IR) spectra were recorded on an Excalibur FTS 4000 setup equipped with a “golden gate”. A lyophilized powder of a peptide amphiphile was placed on top of the crystal and a spectrum was recorded (512 scans at 2 cm^{-1} aperture). Deconvolution and

fitting of the Amide I peaks to the Lorenz function were performed using Origin Pro.

2.5.7 Transmission electron microscopy

For transmission electron microscopy (TEM) measurements, a 10 µL droplet of the sample was placed on a continuous carbon grid on a copper support (200 mesh) and left for 20 secs. The excess liquid was removed by manually blotting with filter paper. The grid was washed with deionized water once and blotted again. Uranyl acetate staining (0.5% w/v) was applied, followed immediately by blotting. Images were collected on a JEM1400 Plus (JEOL) transmission electron microscope operated at 80 kV and equipped with a CCD camera.

2.6 References

1. Goodman, C. M.; McCusker, C. D.; Yilmaz, T.; Rotello, V. M., Toxicity of gold nanoparticles functionalized with cationic and anionic side chains. *Bioconjugate Chem* **2004,** *15* (4), 897-900.

2. Bhamidipati, M.; Fabris, L., Multiparametric Assessment of Gold Nanoparticle Cytotoxicity in Cancerous and Healthy Cells: The Role of Size, Shape, and Surface Chemistry. *Bioconjugate Chem* **2017,** *28* (2), 449-460.

3. Bogliotti, N.; Oberleitner, B.; Di-Cicco, A.; Schmidt, F.; Florent, J. C.; Semetey, V., Optimizing the formation of biocompatible gold nanorods for cancer research: Functionalization, stabilization and purification. *J Colloid Interf Sci* **2011,** *357* (1), 75-81.

4. Schulz, F.; Friedrich, W.; Hoppe, K.; Vossmeyer, T.; Weller, H.; Lange, H., Effective PEGylation of gold nanorods. *Nanoscale* **2016,** *8* (13), 7296-7308.

5. Fytianos, K.; Rodriguez-Lorenzo, L.; Clift, M. J. D.; Blank, F.; Vanhecke, D.; von Garnier, C.; Petri-Fink, A.; Rothen-Rutishauser, B., Uptake efficiency of surface modified gold nanoparticles does not correlate with functional changes and cytokine secretion in human dendritic cells in vitro. *Nanomed-Nanotechnol* **2015,** *11* (3), 633-644.

6. Liu, S. H.; Han, M. Y., Silica-Coated Metal Nanoparticles. *Chem-Asian J* **2010,** *5* (1), 36-45.

7. Hanske, C.; Sanz-Ortiz, M. N.; Liz-Marzan, L. M., Silica-Coated Plasmonic Metal Nanoparticles in Action. *Adv Mater* **2018,** *30* (27): e1707003.

8. Knowles, B. R.; Yang, D.; Wagner, P.; Maclaughlin, S.; Higgins, M. J.; Molino, P. J., Zwitterion Functionalized Silica Nanoparticle Coatings: The Effect of Particle Size on Protein, Bacteria, and Fungal Spore Adhesion. *Langmuir* **2019,** *35* (5), 1335-1345.

9. Sakellari, G. I.; Hondow, N.; Gardiner, P. H. E., Factors influencing the surface functionalization of citrate stabilizaed gold nanoparticles with cysteamine, 3-mercaptopropionic acid or L-selenocysteine for sensor applications. *Chemosensors* **2020,** *8* (3): e80.

10. Gupta, A.; Moyano, D. F.; Parnsubsakul, A.; Papadopoulos, A.; Wang, L. S.; Landis, R. F.; Das, R.; Rotello, V. M., Ultrastable and Biofunctionalizable Gold Nanoparticles. *Acs Appl Mater Inter* **2016,** *8* (22), 14096-14101.

11. Levy, R.; Thanh, N. T. K.; Doty, R. C.; Hussain, I.; Nichols, R. J.; Schiffrin, D. J.; Brust, M.; Fernig, D. G., Rational and combinatorial design of peptide capping Ligands for gold nanoparticles. *J Am Chem Soc* **2004,** *126* (32), 10076-10084.

12. Mei, B. C.; Oh, E.; Susumu, K.; Farrell, D.; Mountziaris, T. J.; Mattoussi, H., Effects of Ligand Coordination Number and Surface Curvature on the Stability of Gold Nanoparticles in Aqueous Solutions. *Langmuir* **2009,** *25* (18), 10604-10611.

13. Shaw, C. P.; Middleton, D. A.; Volk, M.; Levy, R., Amyloid-derived peptide forms self-assembled monolayers on gold nanoparticle with a curvature-dependent beta-sheet structure. *ACS Nano* **2012,** *6* (2), 1416-26.

14. Colangelo, E.; Chen, Q.; Davidson, A. M.; Paramelle, D.; Sullivan, M. B.; Volk, M.; Levy, R., Computational and Experimental Investigation of the Structure of Peptide Monolayers on Gold Nanoparticles. *Langmuir* **2017,** *33* (1), 438-449.

15. Hendricks, M. P.; Sato, K.; Palmer, L. C.; Stupp, S. I., Supramolecular Assembly of Peptide Amphiphiles. *Acc Chem Res* **2017,** *50* (10), 2440-2448.

16. Dreher, M. R.; Simnick, A. J.; Fischer, K.; Smith, R. J.; Patel, A.; Schmidt, M.; Chilkoti, A., Temperature triggered self-assembly of polypeptides into multivalent spherical micelles. *J Am Chem Soc* **2008,** *130* (2), 687-694.

17. Boyle, A. L.; Rabe, M.; Crone, N. S. A.; Rhys, G. G.; Soler, N.; Voskamp, P.; Pannu, N. S.; Kros, A., Selective coordination of three transition metal ions within a coiled-coil peptide scaffold. *Chem Sci* **2019,** *10* (31), 7456-7465.

18. Pashuck, E. T.; Cui, H.; Stupp, S. I., Tuning supramolecular rigidity of peptide fibers through molecular structure. *J Am Chem Soc* **2010,** *132* (17), 6041-6046.

19. Hamley, I. W.; Kirkham, S.; Dehsorkhi, A.; Castelletto, V.; Reza, M.; Ruokolainen, J., Toll-like receptor agonist lipopeptides self-assemble into distinct nanostructures. *Chem Commun (Camb)* **2014,** *50* (100), 15948-15951.

20. Behanna, H. A.; Donners, J. J. J. M.; Gordon, A. C.; Stupp, S. I., Coassembly of amphiphiles with opposite peptide polarities into nanofibers. *J Am Chem Soc* **2005,** *127* (4), 1193-1200.

21. Paramonov, S. E.; Jun, H. W.; Hartgerink, J. D., Self-assembly of peptide-amphiphile nanofibers: the roles of hydrogen bonding and amphiphilic packing. *J Am Chem Soc* **2006,** *128* (22), 7291-7298.

22. Malkar, N. B.; Lauer-Fields, J. L.; Juska, D.; Fields, G. B., Characterization of peptide-amphiphiles possessing cellular activation sequences. *Biomacromolecules* **2003,** *4* (3), 518-528.

23. Hamley, I. W., Self-assembly of amphiphilic peptides. *Soft Matter* **2011,** *7* (9), 4122-4138.

24. Booth, R.; Insua, I.; Bhak, G.; Montenegro, J., Self-assembled microfibres by oxime connection of linear peptide amphiphiles. *Org Biomol Chem* **2019,** *17* (7), 1984-1991.

25. Elgersma, R. C.; Meijneke, T.; de Jong, R.; Brouwer, A. J.; Posthuma, G.; Rijkers, D. T.; Liskamp, R. M., Synthesis and structural investigations of N-alkylated beta-peptidosulfonamide-peptide hybrids of the amyloidogenic amylin(20-29) sequence: Implications of supramolecular folding for the design of peptide-based bionanomaterials. *Org Biomol Chem* **2006,** *4* (19), 3587-3597.

26. Dasgupta, A.; Das, D., Designer Peptide Amphiphiles: Self-Assembly to Applications. *Langmuir* **2019,** *35* (33), 10704-10724.

27. da Silva, R. M. P.; van der Zwaag, D.; Albertazzi, L.; Lee, S. S.; Meijer, E. W.; Stupp, S. I., Super-resolution microscopy reveals structural diversity in molecular exchange among peptide amphiphile nanofibres. *Nat Commun* **2016,** *7*: e11561.

28. Newcomb, C. J.; Sur, S.; Ortony, J. H.; Lee, O. S.; Matson, J. B.; Boekhoven, J.; Yu, J. M.; Schatz, G. C.; Stupp, S. I., Cell death versus cell survival instructed by supramolecular cohesion of nanostructuresl. *Nat Commun* **2014,** *5*: e3321.

29. Newcomb, C. J.; Bitton, R.; Velichko, Y. S.; Snead, M. L.; Stupp, S. I., The Role of Nanoscale Architecture in Supramolecular Templating of Biomimetic Hydroxyapatite Mineralization. *Small* **2012,** *8* (14), 2195-2202.

30. Cote, Y.; Fu, I. W.; Dobson, E. T.; Goldberger, J. E.; Nguyen, H. D.; Shen, J. K., Mechanism of the pH-Controlled Self-Assembly of Nanofibers from Peptide Amphiphiles. *J Phys Chem C Nanomater Interfaces* **2014,** *118* (29), 16272-16278.

31. Cui, H.; Muraoka, T.; Cheetham, A. G.; Stupp, S. I., Self-assembly of giant peptide nanobelts. *Nano Lett* **2009,** *9* (3), 945-51.

32. Cui, H. G.; Cheetham, A. G.; Pashuck, E. T.; Stupp, S. I., Amino Acid Sequence in Constitutionally Isomeric Tetrapeptide Amphiphiles Dictates Architecture of One-Dimensional Nanostructures. *J Am Chem Soc* **2014,** *136* (35), 12461-12468.

33. Tantakitti, F.; Boekhoven, J.; Wang, X.; Kazantsev, R. V.; Yu, T.; Li, J. H.; Zhuang, E.; Zandi, R.; Ortony, J. H.; Newcomb, C. J.; Palmer, L. C.; Shekhawat, G. S.; de la Cruz, M. O.; Schatz, G. C.; Stupp, S. I., Energy landscapes and functions of supramolecular systems. *Nat Mater* **2016,** *15* (4), 469-476.

34. Greenfield, M. A.; Hoffman, J. R.; de la Cruz, M. O.; Stupp, S. I., Tunable Mechanics of Peptide Nanofiber Gels. *Langmuir* **2010,** *26* (5), 3641-3647.

35. Preslar, A. T.; Lilley, L. M.; Sato, K.; Zhang, S. R.; Chia, Z. K.; Stupp, S. I.; Meade, T. J., Calcium-Induced Morphological Transitions in Peptide Amphiphiles Detected by F-19-Magnetic Resonance Imaging. *ACS Appl Mater Inter* **2017,** *9* (46), 39890-39894.

36. Edwards-Gayle, C. J. C.; Hamley, I. W., Self-assembly of bioactive peptides, peptide conjugates, and peptide mimetic materials. *Org Biomol Chem* **2017,** *15* (28), 5867-5876.

37. Tayi, A. S.; Pashuck, E. T.; Newcomb, C. J.; McClendon, M. T.; Stupp, S. I., Electrospinning Bioactive Supramolecular Polymers from Water. *Biomacromolecules* **2014,** *15* (4), 1323-1327.

38. Moyer, T. J.; Finbloom, J. A.; Chen, F.; Toft, D. J.; Cryns, V. L.; Stupp, S. I., pH and Amphiphilic Structure Direct Supramolecular Behavior in Biofunctional Assemblies. *J Am Chem Soc* **2014,** *136* (42), 14746-14752.

39. Xu, X. D.; Jin, Y.; Liu, Y.; Zhang, X. Z.; Zhuo, R. X., Self-assembly behavior of peptide amphiphiles (PAs) with different length of hydrophobic alkyl tails. *Colloid Surface B* **2010,** *81* (1), 329-335.

40. Kelly, S. M.; Price, N. C., The application of circular dichroism to studies of protein folding and unfolding. *Biochim Biophys Acta* **1997,** *1338* (2), 161-185.

41. Greenfield, N. J., Using circular dichroism spectra to estimate protein secondary structure. *Nat Protoc* **2006,** *1* (6), 2876-2890.

42. Berova N., N. K., Woody R., *Circular Dichroism: Principles and Applications*. Wiley-VCH: New York, 2000.

43. Ferreira, D. S.; Marques, A. P.; Reis, R. L.; Azevedo, H. S., Hyaluronan and self-assembling peptides as building blocks to reconstruct the extracellular environment in skin tissue. *Biomater Sci-Uk* **2013,** *1* (9), 952-964.

44. Chirgadze, Y. N.; Nevskaya, N. A., Infrared-Spectra and Resonance Interaction of Amide-One Vibration of Parallel-Chain Pleated Sheet. *Biopolymers* **1976,** *15* (4), 627-636.

45. Susi, H.; Byler, D. M., Resolution-Enhanced Fourier-Transform Infrared-Spectroscopy of Enzymes. *Method Enzymol* **1986,** *130*, 290-311.

46. Venyaminov, S. Y.; Kalnin, N. N., Quantitative Ir Spectrophotometry of Peptide Compounds in Water (H2o) Solutions .1. Spectral Parameters of Amino-Acid Residue Absorption-Bands. *Biopolymers* **1990,** *30* (13-14), 1243-1257.

47. Rozenberg, M.; Shoham, G., FTIR spectra of solid poly-l-lysine in the stretching NH mode range. *Biophys Chem* **2007,** *125* (1), 166-171.

48. Newcomb, C. J.; Moyer, T. J.; Lee, S. S.; Stupp, S. I., Advances in cryogenic transmission electron microscopy for the characterization of dynamic self-assembling nanostructures. *Curr Opin Colloid In* **2012,** *17* (6), 350-359.

2.7 Supporting Information

Purity and identity of all 25 molecules used in this study was determined using LC-MS:

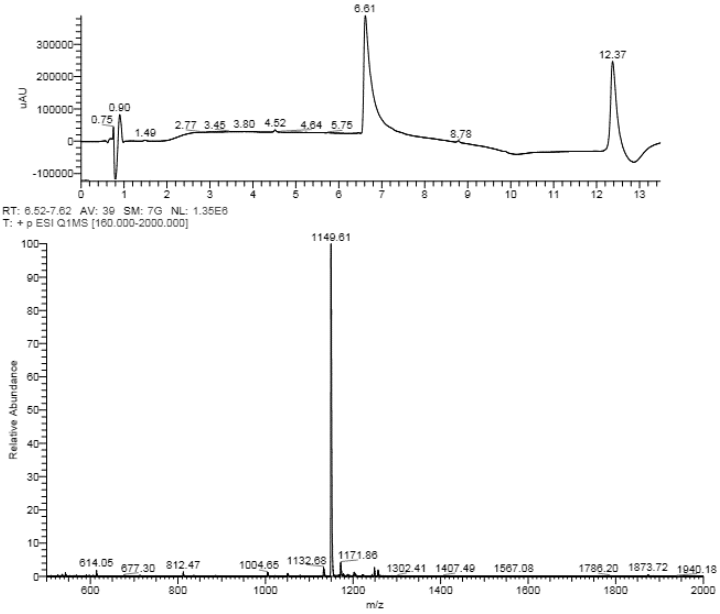

Figure S2.1. LC-MS spectrum of **16-V_3A_3**. $[M+H]^{1+}_{theor}$ = 1149.86.

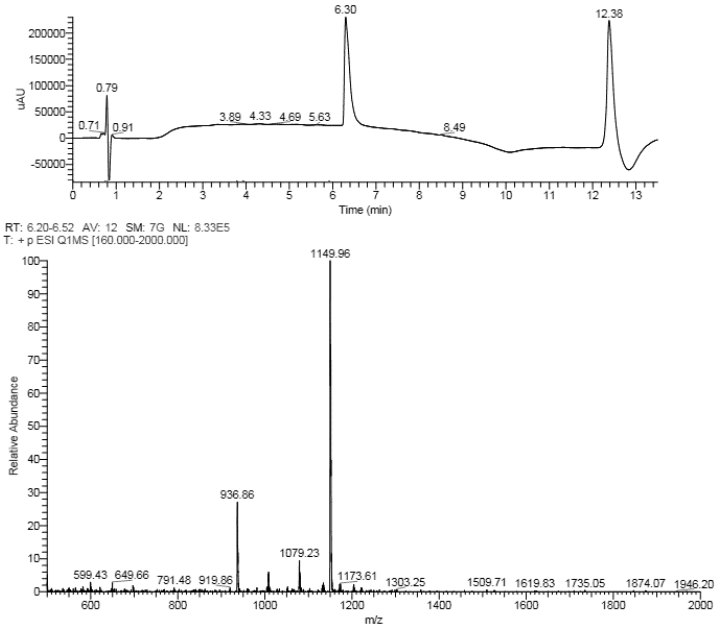

Figure S2.2. LC-MS spectrum of **16-A_3V_3**. $[M+H]^{1+}_{theor}$ = 1149.86.

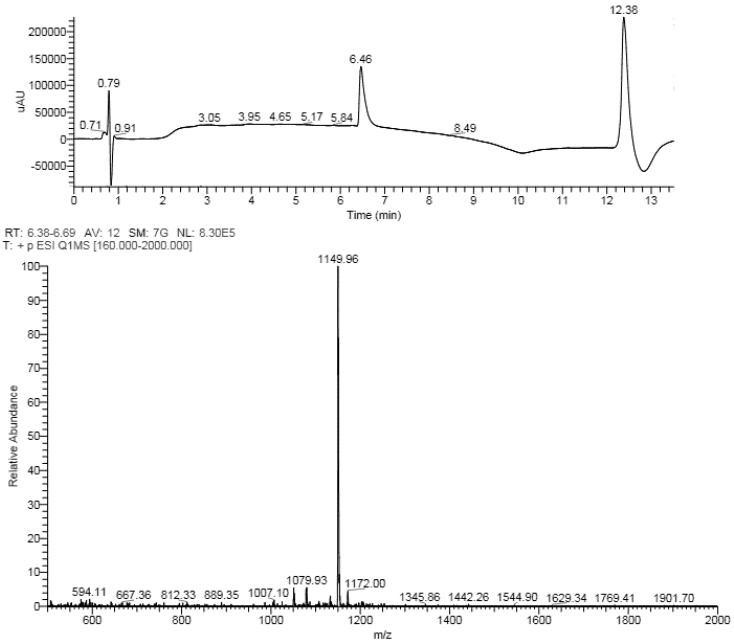

Figure S2.3. LC-MS spectrum of **16-$(VA)_3$**. $[M+H]^{1+}_{theor}$ = 1149.86.

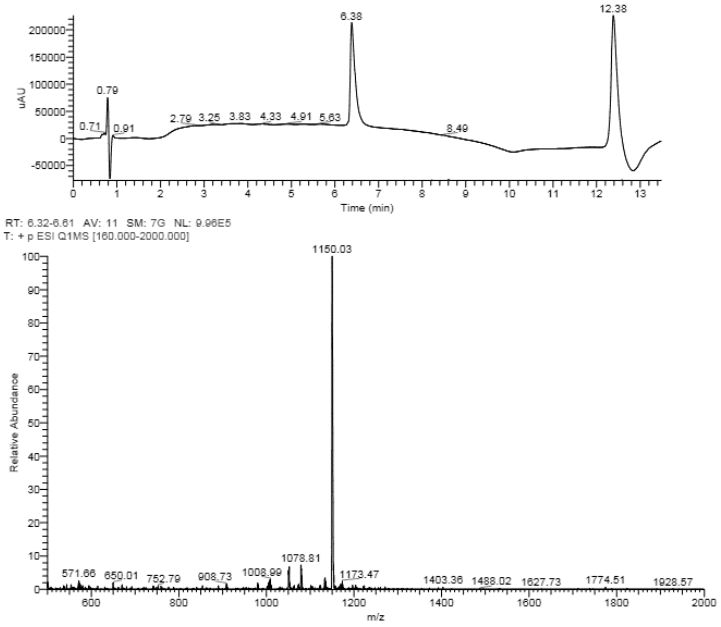

Figure S2.4. LC-MS spectrum of **16-(AV)$_3$**. $[M+H]^{1+}_{theor}$ = 1149.86.

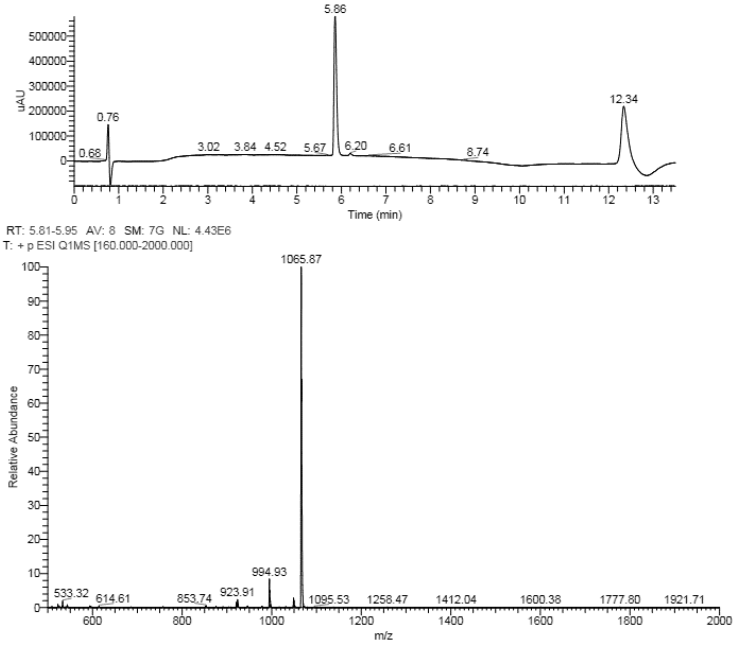

Figure S2.5. LC-MS spectrum of **16-A$_6$**. $[M+H]^{1+}_{theor}$ = 1065.76.

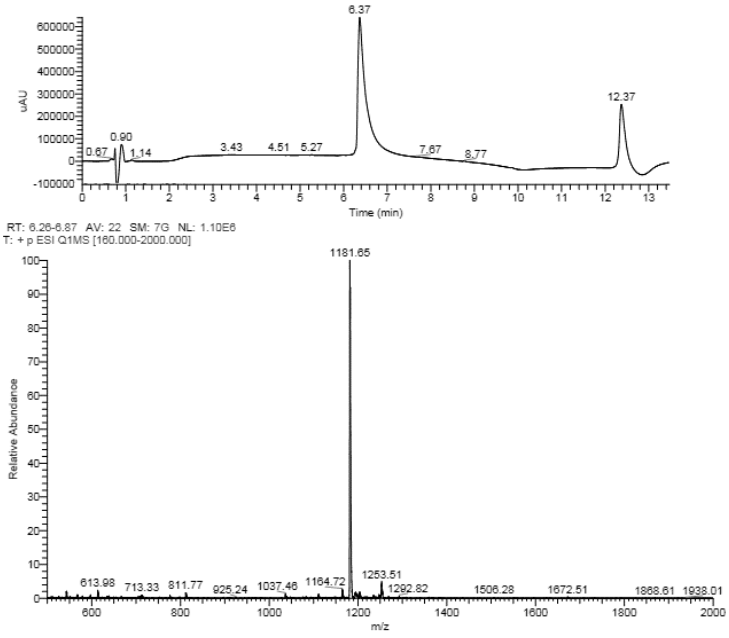

Figure S2.6. LC-MS spectrum of **HS16-V$_3$A$_3$**. $[M+H]^{1+}_{theor}$ = 1181.83.

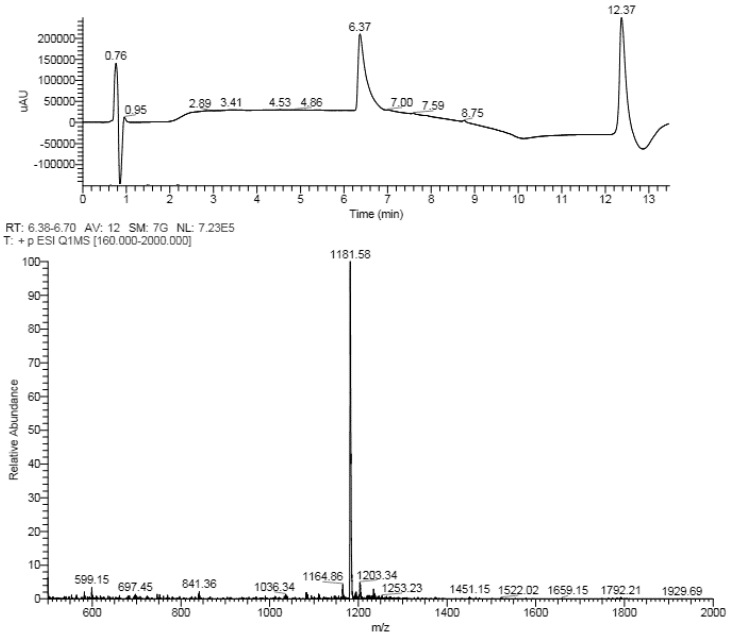

Figure S2.7. LC-MS spectrum of **HS16-A$_3$V$_3$**. $[M+H]^{1+}_{theor}$ = 1181.83.

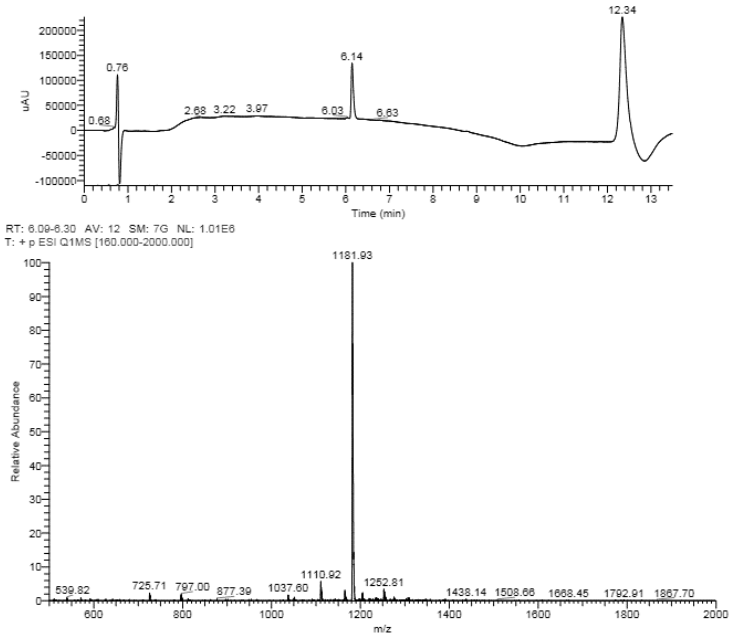

Figure S2.8. LC-MS spectrum of **HS16-(VA)$_3$**. $[M+H]^{1+}_{theor}$ = 1181.83.

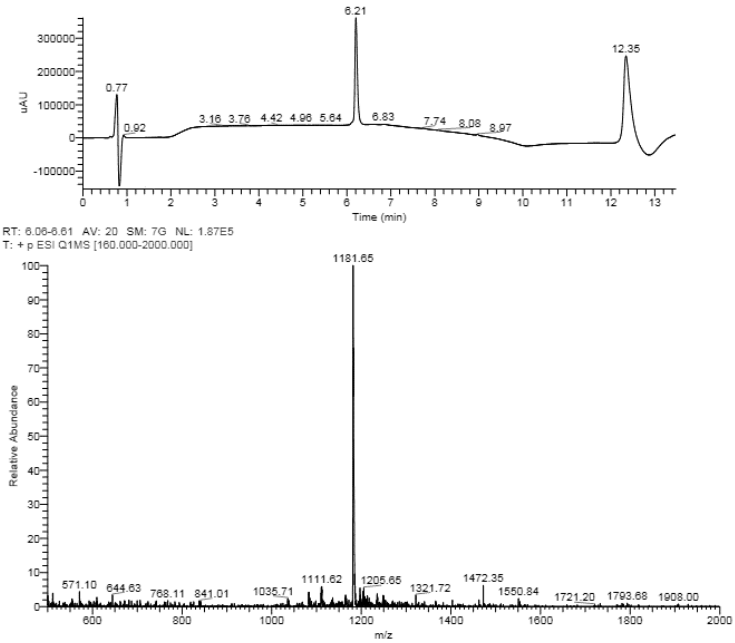

Figure S2.9. LC-MS spectrum of **HS16-(AV)$_3$**. $[M+H]^{1+}_{theor}$ = 1181.83.

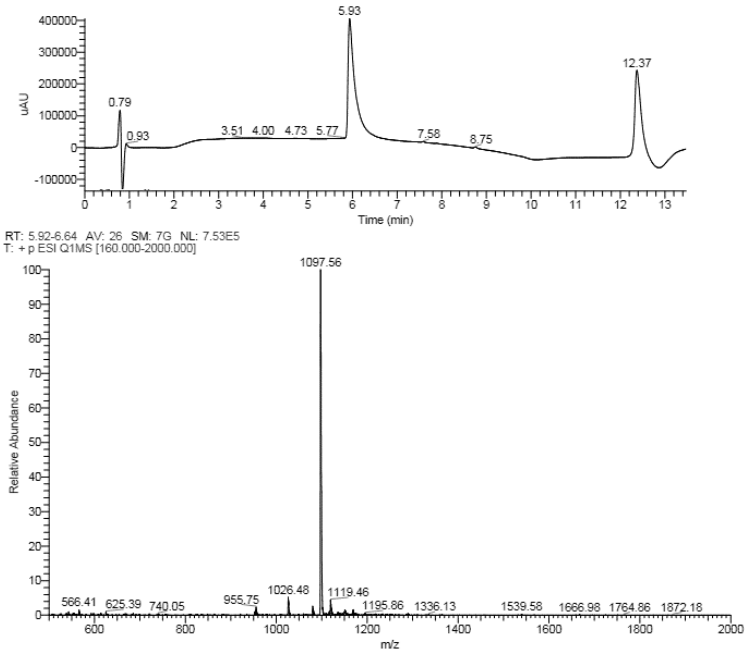

Figure S2.10. LC-MS spectrum of **HS16-A$_6$**. $[M+H]^{1+}_{theor}$ = 1097.74.

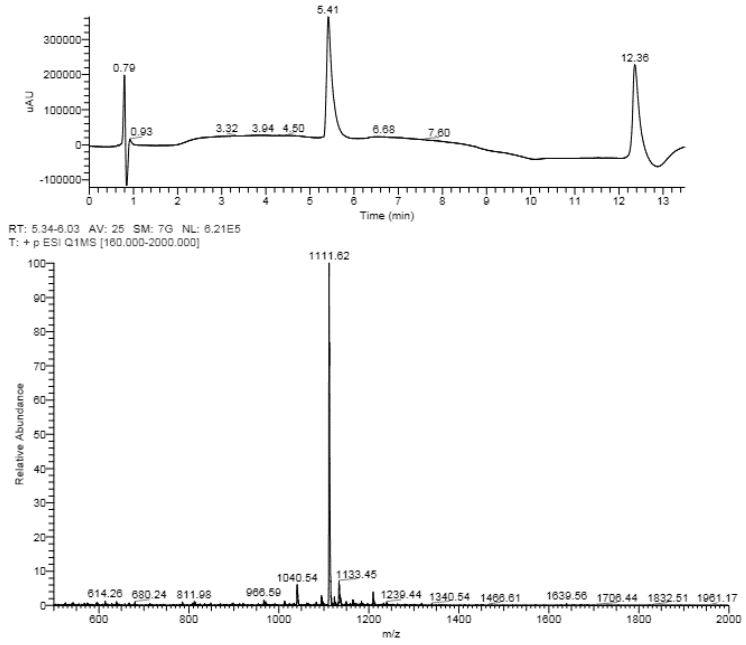

Figure S2.11. LC-MS spectrum of **HS11-V$_3$A$_3$**. $[M+H]^{1+}_{theor}$ = 1111.75.

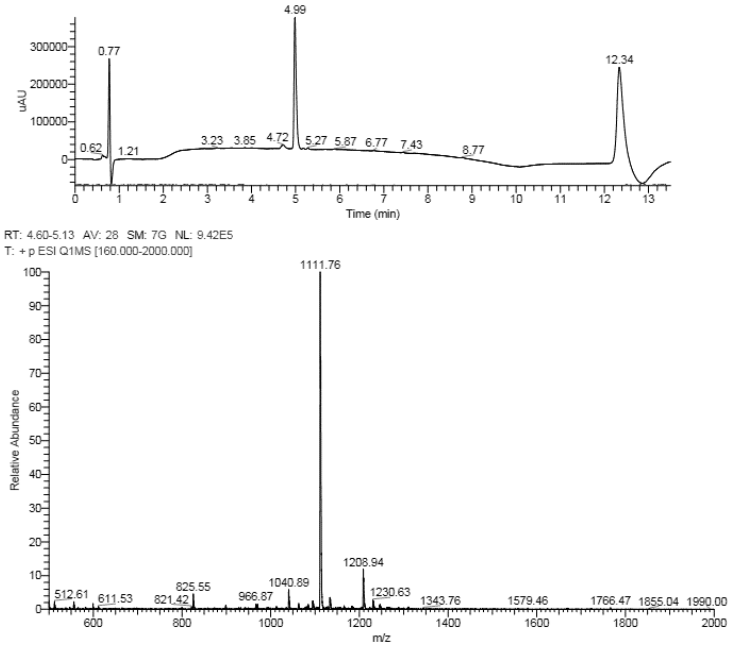

Figure S2.12. LC-MS spectrum of **HS11-A_3V_3**. $[M+H]^{1+}_{theor}$ = 1111.75.

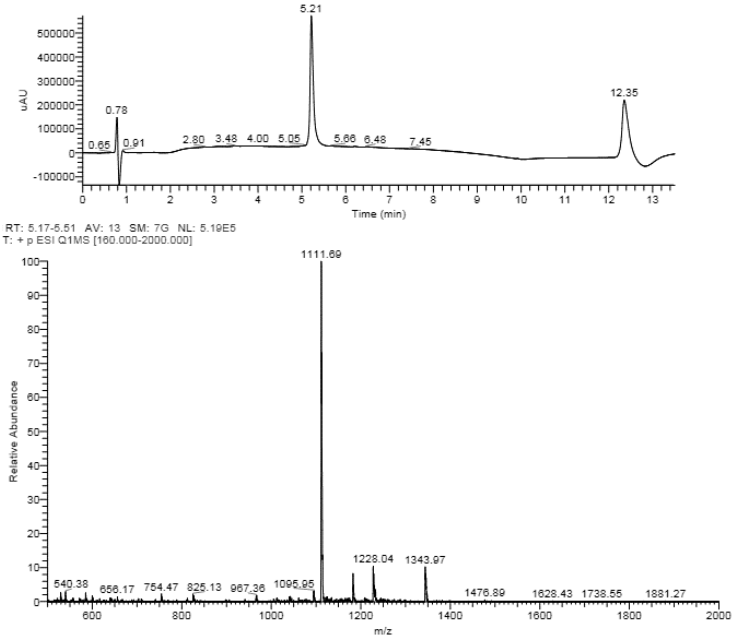

Figure S2.13. LC-MS spectrum of **HS11-$(VA)_3$**. $[M+H]^{1+}_{theor}$ = 1111.75.

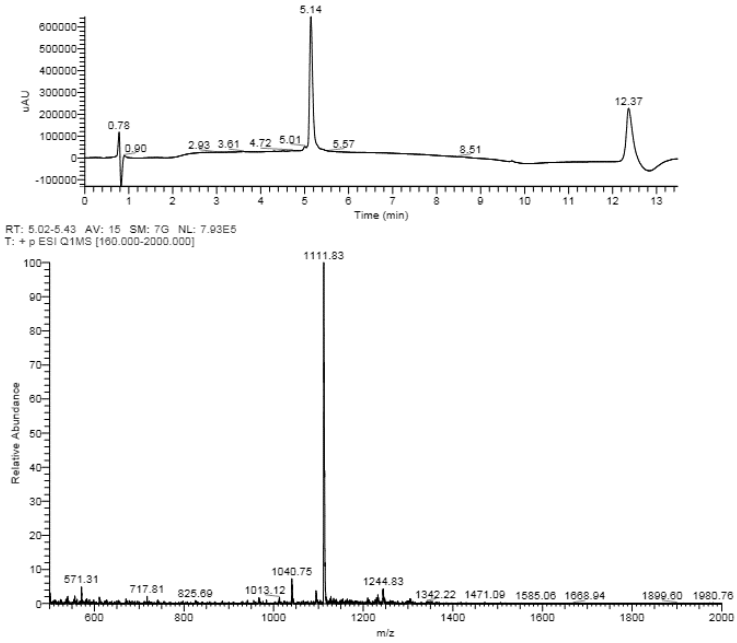

Figure S2.14. LC-MS spectrum of **HS11-(AV)$_3$**. $[M+H]^{1+}_{theor}$ = 1111.75.

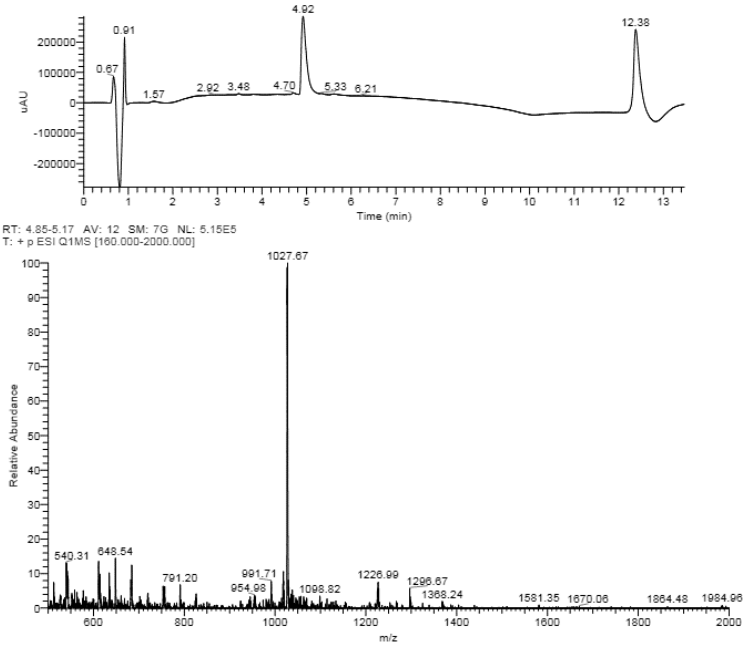

Figure S2.15. LC-MS spectrum of **HS11-A$_6$**. $[M+H]^{1+}_{theor}$ = 1027.66.

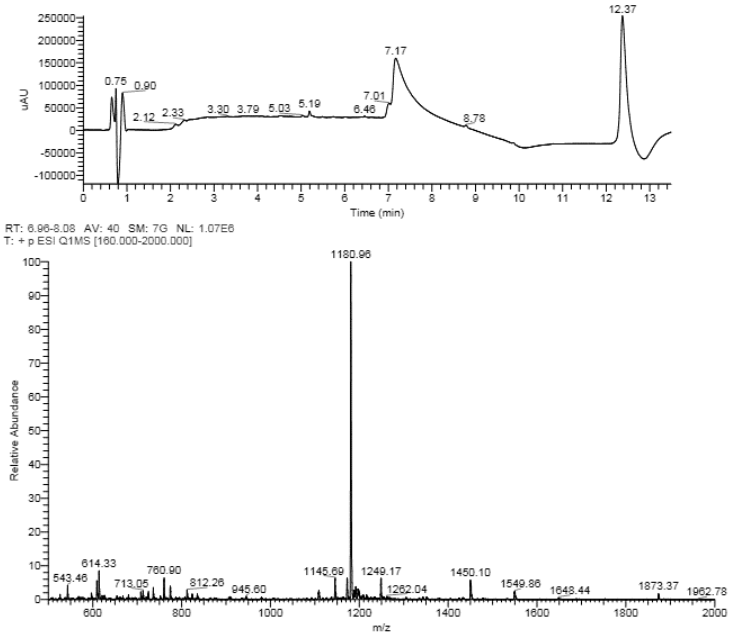

Figure S2.16. LC-MS spectrum of **di-16-V_3A_3**. $[M+2H]^{2+}_{theor}$ = 1181.33.

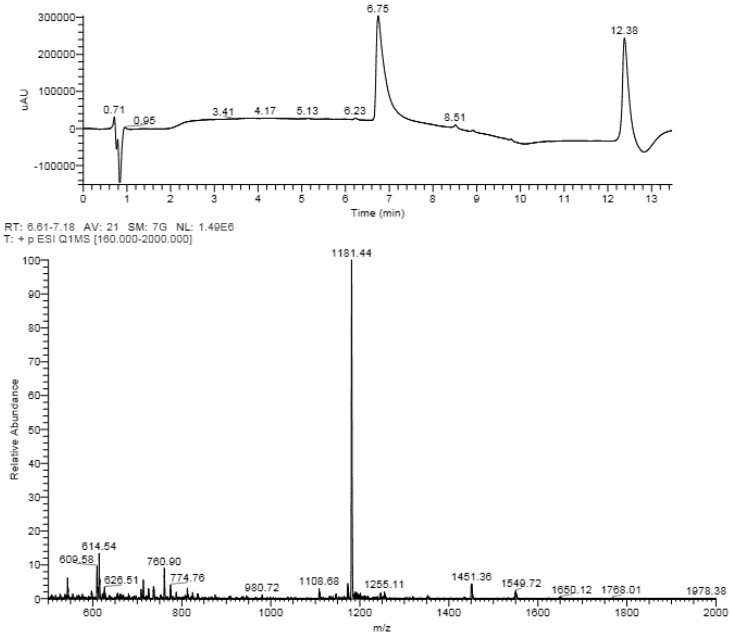

Figure S2.17. LC-MS spectrum of **di-16-A_3V_3**. $[M+2H]^{2+}_{theor}$ = 1181.33.

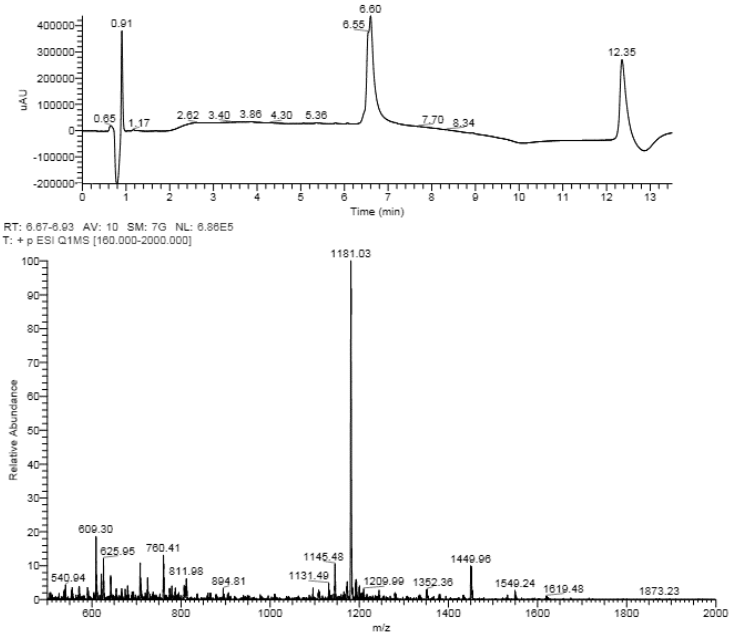

Figure S2.18. LC-MS spectrum of **di-16-(VA)$_3$**. $[M+2H]^{2+}_{theor}$ = 1181.33.

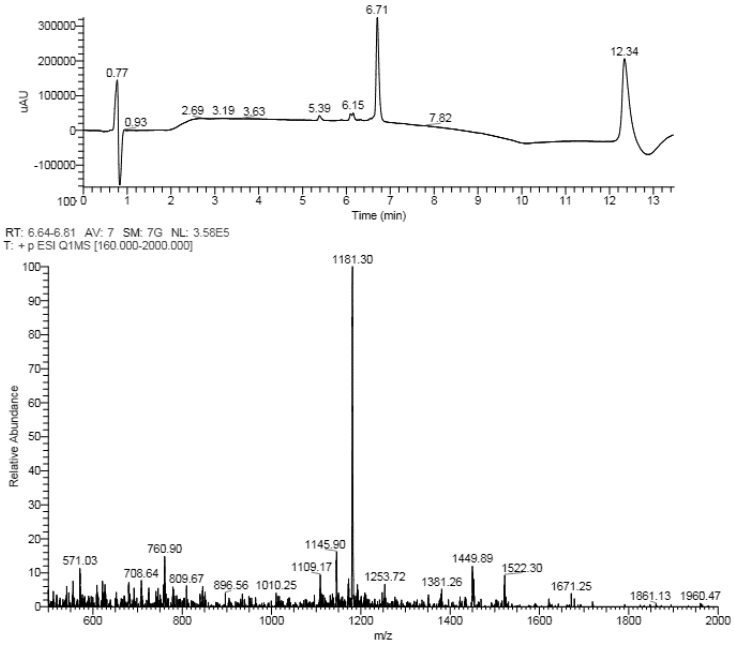

Figure S2.19. LC-MS spectrum of **di-16-(AV)$_3$**. $[M+2H]^{2+}_{theor}$ = 1181.33.

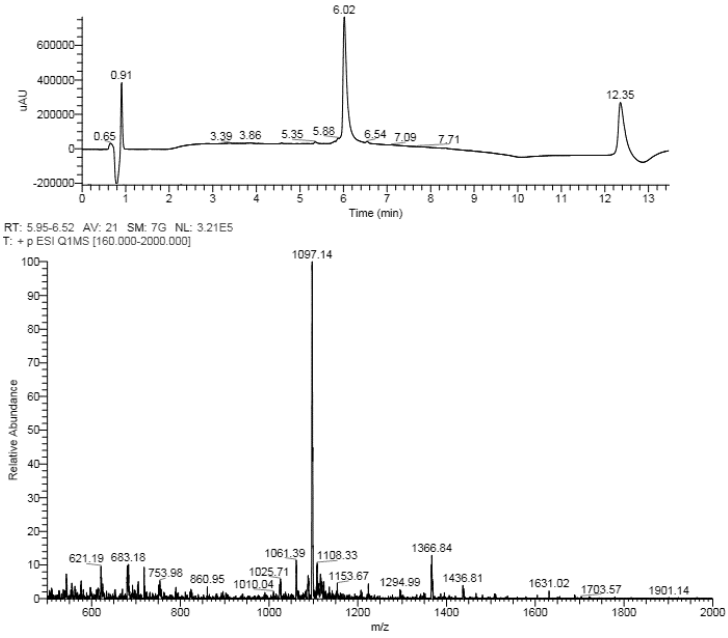

Figure S2.20. LC-MS spectrum of **di-16-A$_6$**. $[M+2H]^{2+}_{theor}$ = 1097.23.

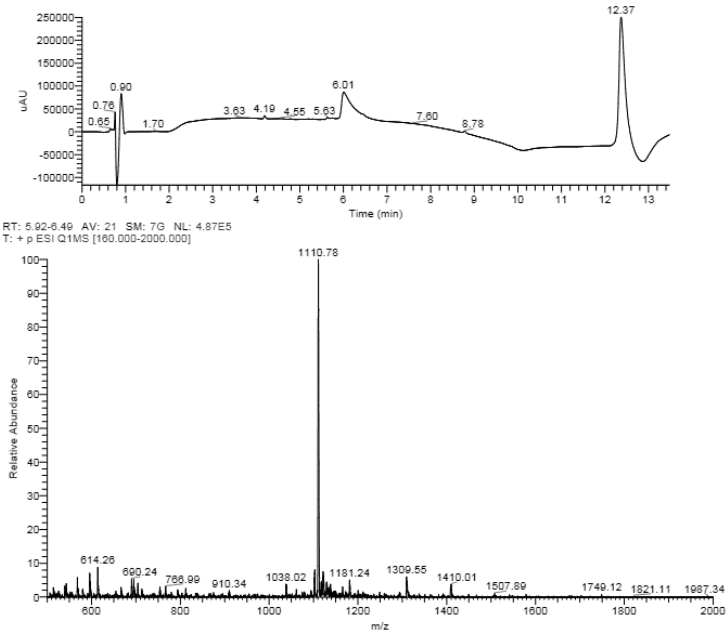

Figure S2.21. LC-MS spectrum of **di-11-V$_3$A$_3$**. $[M+2H]^{2+}_{theor}$ = 1181.33.

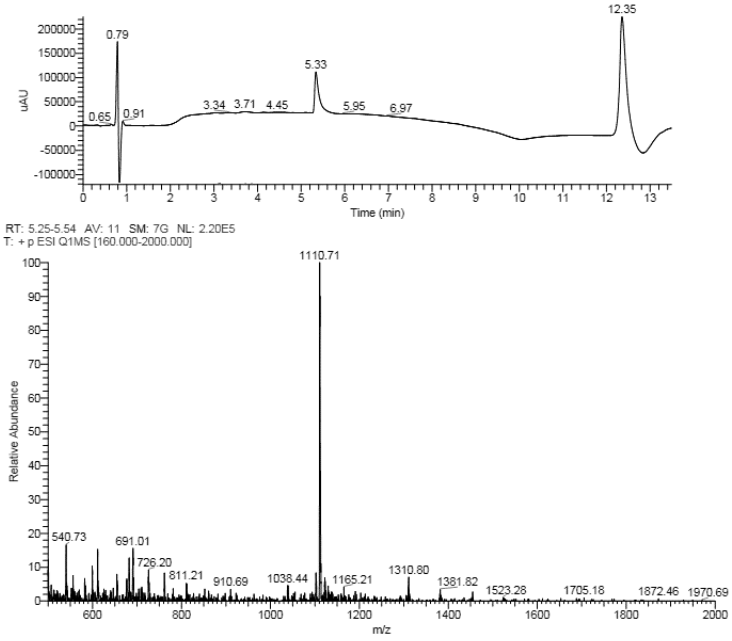

Figure S2.22. LC-MS spectrum of **di-11-A_3V_3**. $[M+2H]^{2+}_{theor}$ = 1111.25.

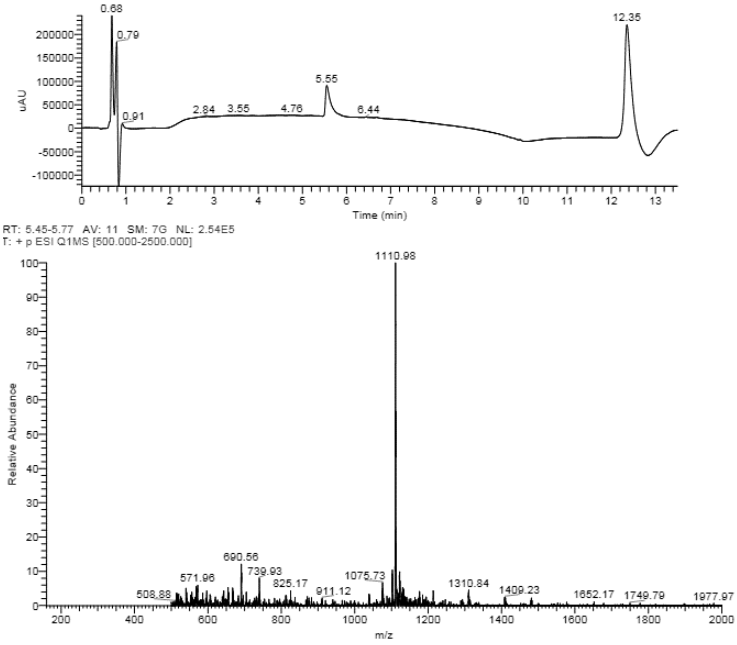

Figure S2.23. LC-MS spectrum of **di-11-$(VA)_3$**. $[M+2H]^{2+}_{theor}$ = 1111.25.

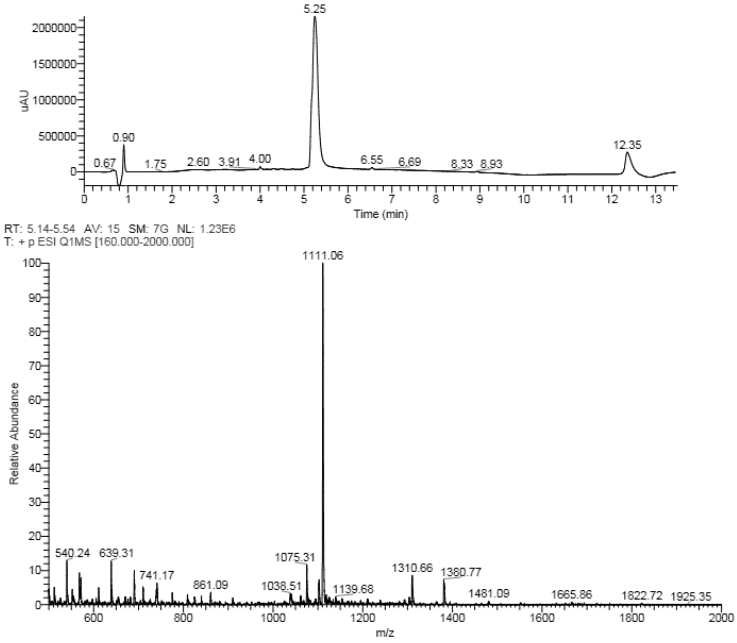

Figure S2.24. LC-MS spectrum of **di-11-(AV)$_3$**. $[M+2H]^{2+}_{theor}$ = 1111.25.

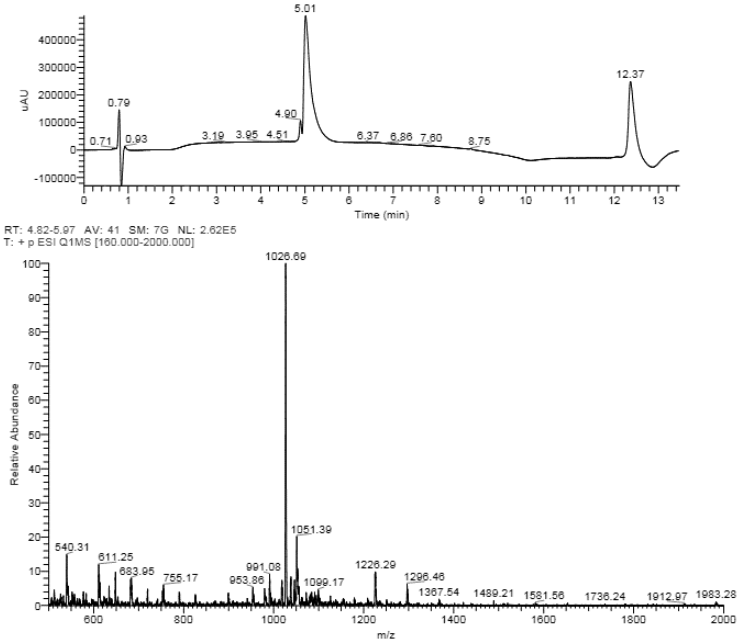

Figure S2.25. LC-MS spectrum of **di-11-A$_6$**. $[M+2H]^{2+}_{theor}$ = 1027.15.

Spontaneous oxidation of peptide amphiphile thiol groups:

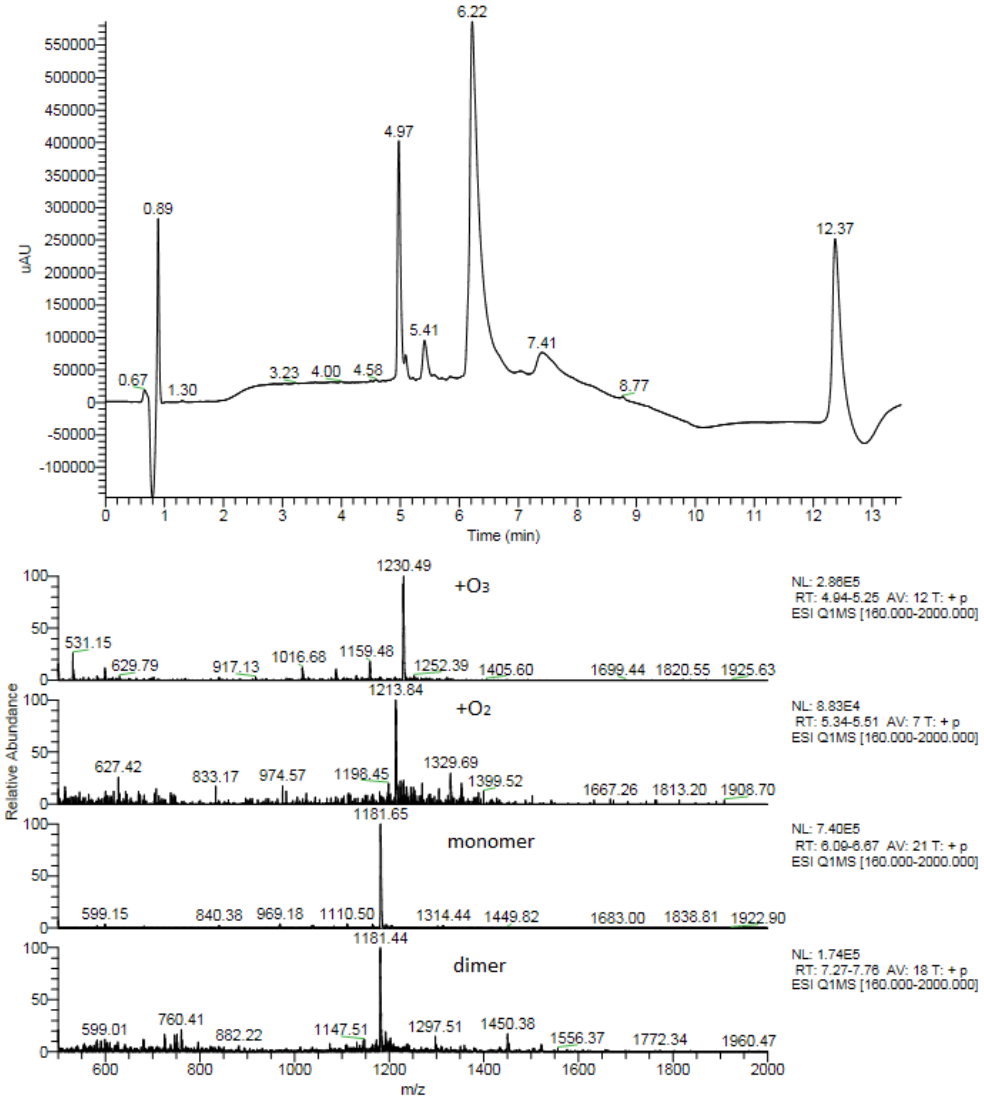

Figure S2.26. LC-MS spectra of **HS16-A$_3$V$_3$** after long-term storage in the lyophilized state at +4 ºC (~1 year). Oxidation of the terminal thiol gave rise to a dimeric species, as well as +O_2 and +O_3.

Secondary structure profiling based on Amide I fitting:

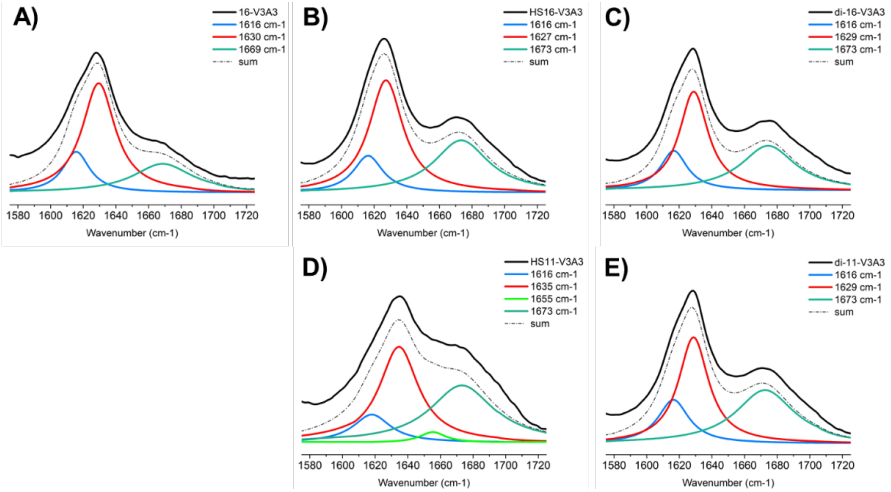

Figure S2.27. Fitting of the Amide I peak for peptide amphiphiles bearing the **V_3A_3** peptide domain: blue line represents the terminal amide; red line - the joint contribution of β-structures and amino groups of Lys residues; green line – α-helices; cyan line – other structures. Each figure shows the same peptide domain coupled to different alkyl chains: (A) **16-**, (B) **HS16-**, (C) **di-16-**, (D) **HS11-**, (E) and **di-11-**.

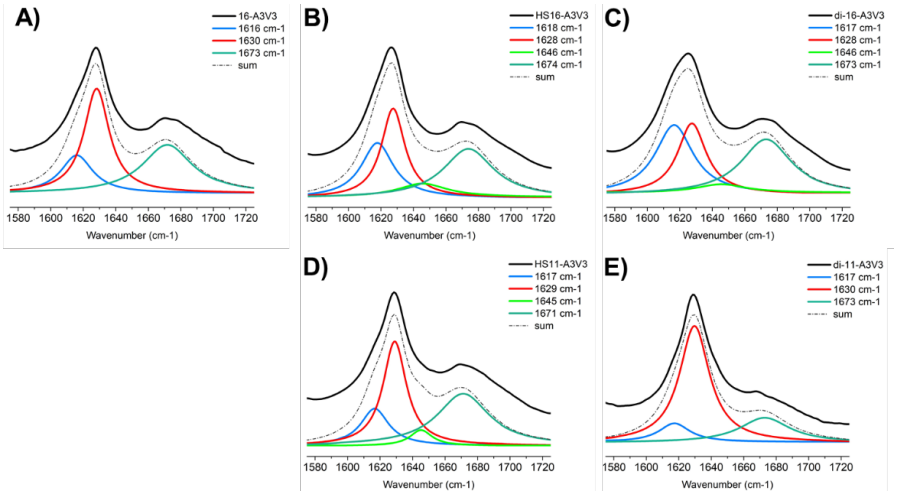

Figure S2.28. Fitting of the Amide I peak for peptide amphiphiles bearing the **A_3V_3** peptide domain: blue line represents the terminal amide; red line - the joint contribution of β-structures and amino groups of Lys residues; green line – α-helices; cyan line – other structures. Each figure shows the same peptide domain coupled to different alkyl chains: (A) **16-**, (B) **HS16-**, (C) **di-16-**, (D) **HS11-**, (E) and **di-11-**.

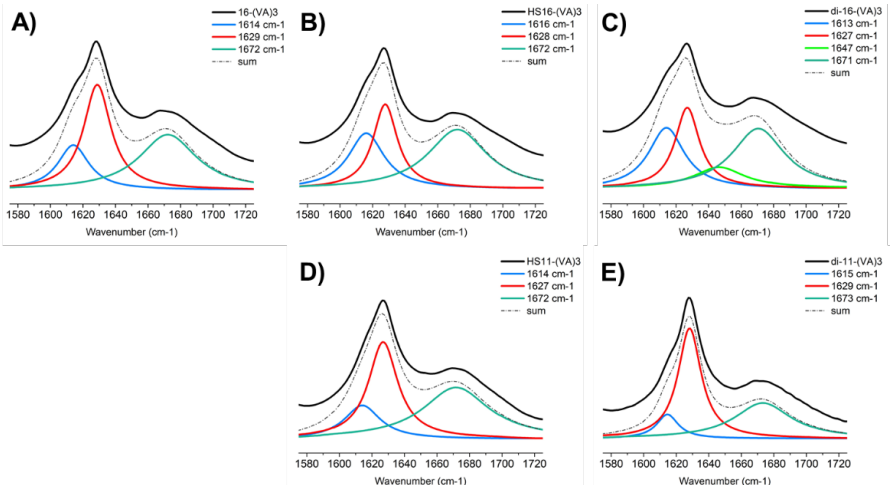

Figure S2.29. Fitting of the Amide I peak for peptide amphiphiles bearing the **$(VA)_3$** peptide domain: blue line represents the terminal amide; red line - the joint contribution of β-structures and amino groups of Lys residues; green line – α-helices; cyan line – other structures. Each figure shows the same peptide domain coupled to different alkyl chains: (A) **16-**, (B) **HS16-**, (C) **di-16-**, (D) **HS11-**, (E) and **di-11-**.

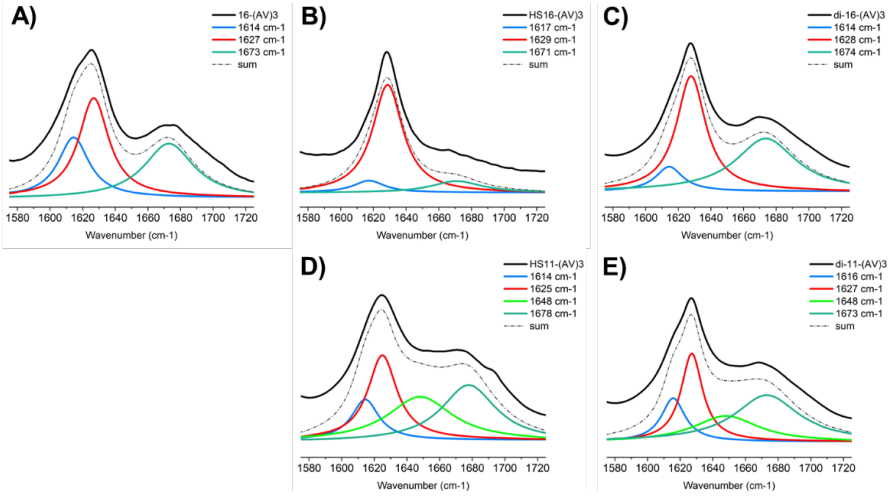

Figure S2.30. Fitting of the Amide I peak for peptide amphiphiles bearing the **$(AV)_3$** peptide domain: blue line represents the terminal amide; red line - the joint contribution of β-structures and amino groups of Lys residues; green line – α-helices; cyan line – other structures. Each figure shows the same peptide domain coupled to different alkyl chains: (A) **16-**, (B) **HS16-**, (C) **di-16-**, (D) **HS11-**, (E) and **di-11-**.

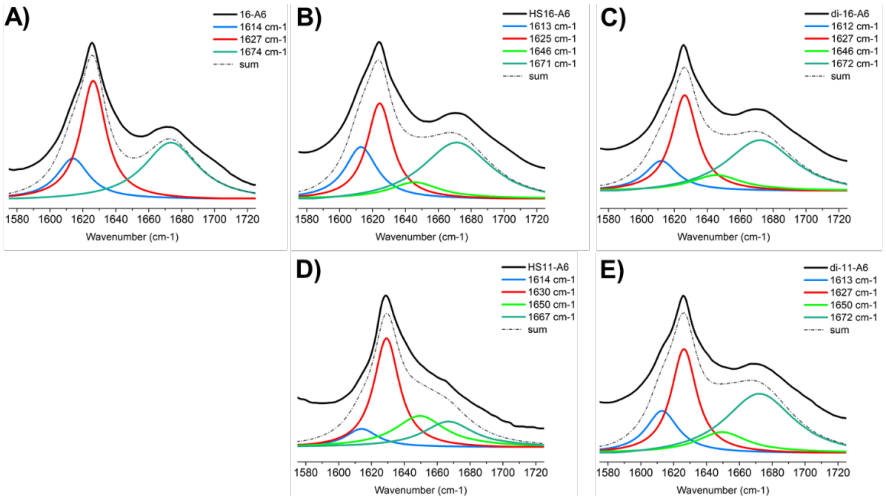

Figure S2.31. Fitting of the Amide I peak for peptide amphiphiles bearing the $\mathbf{A_6}$ peptide domain: blue line represents the terminal amide; red line - the joint contribution of β-structures and amino groups of Lys residues; green line – α-helices; cyan line – other structures. Each figure shows the same peptide domain coupled to different alkyl chains: (A) **16-**, (B) **HS16-**, (C) **di-16-**, (D) **HS11-**, (E) and **di-11-**.